

Discovery of 11 New T Dwarfs in the Two Micron All-Sky Survey, Including a Possible L/T Transition Binary

Dagny L. Looper¹

*Institute for Astronomy, University of Hawai'i, 2680 Woodlawn Dr, Honolulu, HI 96822;
dagny@ifa.hawaii.edu*

J. Davy Kirkpatrick¹

*Infrared Processing and Analysis Center, MS 100-22, California Institute of Technology,
Pasadena, CA 91125*

Adam J. Burgasser¹

*MIT Kavli Institute for Astrophysics & Space Research, 77 Massachusetts Ave, Building
37-664B, Cambridge, MA 02139*

ABSTRACT

We present the discovery of 11 new T dwarfs, found during the course of a photometric survey for mid-to-late T dwarfs in the 2MASS Point Source Catalog and from a proper motion selected sample of ultracool dwarfs in the 2MASS Working Database. Using the NASA Infrared Telescope Facility SpeX spectrograph, we obtained low-resolution ($R \sim 150$) spectroscopy, allowing us to derive near-infrared spectral types of T2–T8. One of these new T dwarfs, 2MASS J13243559+6358284, was also discovered independently by Metchev et al. in prep. . This object is spectroscopically peculiar and possibly a binary and/or very young (< 300 Myr). We specifically attempted to model the spectrum of this source as a composite binary to reproduce its peculiar spectral characteristics. The latest-type object in our sample is a T8 dwarf, 2MASS J07290002–3954043, now one of the four latest-type T dwarfs known. All 11 T dwarfs are nearby given their spectrophotometric distance estimates, with 1 T dwarf within 10 pc and 8 additional T dwarfs within 25 pc, if single. These new additions increase the 25 pc census of T dwarfs by $\sim 14\%$. Their proximity offers an excellent opportunity to probe for companions at closer separations than are possible for more distant T dwarfs.

Subject headings: stars: low-mass, brown dwarfs — techniques: spectroscopic

1. Introduction

The T spectral class (Burgasser et al. 2002; Geballe et al. 2002) is currently the coolest populated class on the MK system, with effective temperatures ranging from ~ 1400 K at the L/T transition down to ~ 700 K for the coolest known T dwarf (Golimowski et al. 2004; Vrba et al. 2004; Kirkpatrick 2005). The transition between the L and T spectral classes is characterized by the onset of CH_4 absorption in the near-infrared. By mid-type T, the spectral class is dominated by CH_4 , H_2O , and collision induced absorption by H_2 (CIA H_2) in the near-infrared (Saumon et al. 1994; Borysow et al. 1997; Kirkpatrick et al. 2006).

Since the discovery of the T prototype Gl 229B (Nakajima et al. 1995; Oppenheimer et al. 1995) in 1995, ~ 100 T dwarfs have been identified². These objects are our coolest neighbors, spanning the mass and temperature gap between giant planets and the lowest mass stars. Unlike extrasolar planets, we can directly image and often spectroscopically observe T dwarfs in the field and as companions to more massive stars. Therefore, these objects offer invaluable testbeds for extrasolar giant planet atmospheric models.

Due to their intrinsic faintness, the census of T dwarfs in the Solar Neighborhood remains largely incomplete. To date, two surveys have provided the largest contributions to the currently known population: the Sloan Digitized Sky Survey (SDSS, York et al. 2000), a wide-field optical survey, and the Two Micron All Sky Survey (2MASS; Skrutskie et al. 2006), a near-infrared all sky survey. T dwarfs emit most of their flux in the near-infrared; however, due to the $J - K_s$ color degeneracy of early-type T dwarfs and M dwarfs, recovery of early-type T dwarfs by the 2MASS survey has proven difficult. The SDSS survey, while successful at identifying early-type (hotter) T dwarfs using far-optical color selections, is not as sensitive to late-type (cooler) T dwarfs, which emit very little flux at visual wavelengths.

To expand the census of the Sun’s coolest neighbors, we have conducted a photometric survey for mid-to-late type T dwarfs using the 2MASS Point Source Catalog, searching both deeper than previous surveys for T dwarfs (Burgasser et al. 1999, 2000a,b, 2002, 2003a,c, 2004b; Tinney et al. 2005; Ellis et al. 2005) as well as in the Galactic Plane. We present the

¹Visiting Astronomer at the Infrared Telescope Facility, which is operated by the University of Hawaii under Cooperative Agreement no. NCC 5-538 with the National Aeronautics and Space Administration, Science Mission Directorate, Planetary Astronomy Program.

²See <http://dwarfarchives.org> for a full list of T dwarfs.

discovery of eight new T dwarfs from this search, including the discovery of a very nearby ($d \sim 8.4$ pc) T8 dwarf. We also present the first three T dwarfs from our 2MASS proper motion search, all of which are early-type T dwarfs. We describe these two searches in §2. In §3, we describe the spectroscopic observations obtained with the NASA Infrared Telescope Facility 3.0 m SpeX spectrograph and the characterization of this new set of T dwarfs. In §4, we discuss the current census of the Solar Neighborhood. Finally, in §5 we give our conclusions.

2. Observations

2.1. Target Selection

The eleven new T dwarfs we report here were discovered in two different searches using Two Micron All Sky Survey (2MASS) data: (1) a 2MASS photometric search for mid-to-late type T dwarfs and (2) a 2MASS proper motion survey for ultracool dwarfs.

2.1.1. 2MASS Photometric Selection of Mid-to-Late Type T Dwarfs

This search was designed to identify mid-to-late type T dwarfs and to be complementary to previous searches by Burgasser et al. using the 2MASS database. Their most recent search selected sources with $|b| \geq 15^\circ$, $J \leq 16.0$, $J-H \leq 0.3$ or $H-K_s \leq 0$, and no optical counterpart within a $5''$ radius in the USNO-A2.0 catalog or by visual inspection of DSS I and II images. We extended our search half a magnitude deeper in J-band for the same area of sky ($|b| \geq 15^\circ$, $16 < J \leq 16.5$) and searched the galactic plane ($|b| < 15^\circ$), a portion of sky completely unexplored by Burgasser et al. We also modified our color selection criteria, described below, to decrease the number of false positives followed-up spectroscopically.

Our search was broken into three parts defined by galactic latitude: (1) $|b| \geq 15^\circ$, (2) $10^\circ \leq |b| < 15^\circ$, and (3) $|b| < 10^\circ$. All three searches had the following keywords (in parentheses) in common –

1. Not a cataloged minor planet at the time the 2MASS Point Source Catalog was constructed (`mp_flg=0`);
2. No contamination by galaxies (`gal_contam=0`);
3. No artifact contamination or source confusion (`cc_flg` like '000');
4. No optical counterpart within a $5''$ radius in the USNO-A2.0 Catalog (`nopt_mchs=0`)

or by visual inspection of DSS II I-band images³;

5. A non-null detection in both J- and H-bands (`j_cmsig` is not null and `h_cmsig` is not null);

6. Sky positions not coincident with the Large Magellanic Cloud, Small Magellanic Cloud, or 47 Tuc.

The J-band magnitude and near-infrared color cuts for each of the three galactic latitude searches are defined in Table 1. For (1) $|b| \geq 15^\circ$ and (2) $10^\circ \leq |b| < 15^\circ$, we used the same color selection ($(J-H \leq 0)$ or $(J-H \leq 0.3$ and $H-K_s \leq 0)$). This color selection is similar but more restrictive than that used by Burgasser et al. (2003a) ($J-H \leq 0$ or $H-K_s \leq 0$) and was modified from that search because of the high incidence of M dwarfs ($\sim 89\%$) and low incidence of T dwarfs in spectroscopic follow-up ($\sim 11\%$, Burgasser et al. 2004b). Burgasser et al. had relaxed color selection criteria to allow detection of early-type T dwarfs ($< T4$). For (3) $|b| < 10^\circ$, we further restricted our color selection ($J-H \leq 0$) and brightness limit ($J \leq 16$) due to the high density of sources in the galactic plane and searched only outside the galactic center, $|l| \geq 20^\circ$. These color selections effectively limited our search to $\text{SpT} > T4$ (see Figure 1).

Of the three searches, the galactic plane search: (3) $|b| < 10^\circ$ and $|l| \geq 20^\circ$, had the lowest rate of transients (40%, asteroids, spurious detections, flare events, etc., see Table 2) and, after confirmation, highest rate of T dwarfs (100%). The three new T dwarfs from this search are 2MASS 0602+40⁴, 2MASS 1007–45, and 2MASS 2154+59 (see Table 3). In comparison, (1) $|b| \geq 15^\circ$ had a transient rate of $\sim 79\%$ and, after confirmation, T dwarf rate of $\sim 58\%$, with 4 new T dwarfs identified: 2MASS 0510–42, 2MASS 1215–34, 2MASS 1615+13, and 2MASS 2154–10 (see Table 3). Three previously known T dwarfs were also recovered: SDSS 1630+08 (T5.5, Chiu et al. 2006), SDSS 1758+46 (T6.5, Knapp et al. 2004), and SDSS 2124+01 (T5, Knapp et al. 2004, see Table 4). The search (2) $10^\circ \leq |b| < 15^\circ$ had a transient rate of $\sim 67\%$ and, after confirmation, a T dwarf rate of 50%, with 1 new T dwarf identified: 2MASS 0729–39 (see Table 3). The lower transient and higher T dwarf rate for the galactic plane search arises from the better photometry ($J \leq 16$) and more restrictive color selection ($J-H \leq 0$) used.

The total incidence of transients in these three searches was $\sim 71\%$. In Figure 2, we show a histogram of the fraction of transients versus ecliptic latitude. The vast majority

³Images acquired from <http://cadwww.dao.nrc.ca/cadcbin/getdss>.

⁴We abbreviate all of our discoveries from “2MASS Jhhmmss[.ss]±ddmmss[.]s” to “2MASS hhmm±dd” in the text for ease of reading but give their full designations in Table 3.

(84%) are located within 30° of the ecliptic. The remaining 16% are likely highly inclined asteroids or image artifacts. We list all 50 transients in Table 2.

By contrast, the 8 newly identified and 3 confirmed T dwarfs are distributed nearly evenly across ecliptic latitude (β ; see Figure 2). For all confirmed candidates, we find a fraction of 0.45 for M dwarfs and 0.55 for T dwarfs, an improvement of five-fold over Burgasser et al.’s search despite more uncertain photometry for $|\beta| \geq 10^\circ$ and $16.0 < J \leq 16.5$. This increased rate of T dwarf detection occurred because our color selection lies further from the locus of M dwarfs, leading to less scattering from uncertain photometry of faint M dwarfs into our color selection (see Figure 1). To date, we have completed follow-up of 67 of 70 candidates visible from IRTF⁵ and have 11 candidates too northerly or southerly to be observed by IRTF. Of these remaining 14 candidates, 11 have $|\beta| > 30^\circ$. Taking into account the photometry and ecliptic latitudes of these remaining sources, we estimate that 4–5 of these remaining candidates are T dwarfs. We have programs on IRTF/Spex, Gemini-North/NIFS, and SOAR/OSIRIS to obtain imaging/spectroscopy of all remaining 14 candidates and will present the results in a future paper.

2.1.2. 2MASS Proper Motion Survey

We have carried out a proper motion survey for ultracool dwarfs using ~ 4700 sq. degrees of multi-epoch data in the 2MASS Working Database. We give a brief outline of the search criteria here and refer the reader to Looper et al. in prep, for full details of this search. For this dataset, we selected all objects with a proper motion exceeding $0''.2 \text{ yr}^{-1}$, a time difference between epochs of $\Delta t \geq 0.2 \text{ yr}$, a positional difference exceeding $0''.4$ between the first and last epochs, and $J \leq 16.5$. We also required no optical counterpart within a $5''$ radius in the USNO-A2.0 catalog (Monet et al. 1998) or by visual inspection of Digitized Sky Survey (DSS) I and II V- or R-band images. For particularly bright objects, we required large R–J colors ($R-J > 6$). This search resulted in ~ 140 candidates. To date, we have spectroscopically followed-up ~ 120 of these objects, and we report on follow-up of three of these objects here: 2MASS 1106+27, 2MASS 1324+63, and 2MASS 1404–31 (see Table 3). 2MASS 1324+63 was independently identified as a T dwarf by Metchev et al. in prep. Both 2MASS 1106+27 and 2MASS 1404–31 are new discoveries. We also identified two previously discovered T dwarfs: 2MASS 0939–24 (T8, Tinney et al. 2005) and SDSSp 1346–00 (T6.5, Tsvetanov et al. 2000, see Table 4).

⁵IRTF: $\sim -48^\circ < \delta \leq +69^\circ 56'$ (hard limit).

2.2. Imaging: UH 2.2m/ULBCAM & IRTF 3.0m/SpeX

We conducted follow-up imaging to cull the large number of transients from our 2MASS photometric search sample, using the UH 2.2m⁶/ULBCAM and the IRTF 3.0m⁶/SpeX cameras. Our 2MASS proper motion search sample did not require follow-up imaging since second epoch 2MASS images confirmed the existence of our targets. We imaged a total of 67 candidates during several runs described below.

The Ultra Low Background Camera (ULBCAM⁷) is a mosaic infrared camera with four 2048×2048 arrays, a $17' \times 17'$ field-of-view (FOV), and a $0''.25$ pixel scale. However, we used only the top right array, with an individual FOV of $8' 32'' \times 8' 32''$, because it has the highest quantum efficiency and lowest number of bad pixels of the four arrays. We imaged candidates with ULBCAM on 09–12 & 16 Feb 2006 UT and 24 Jul 2006 UT with clear and photometric conditions on all nights and good seeing ($\lesssim 1''$ at J-band). We used the J-band filter for all observations and dithered between exposures, where individual exposure times varied from 20 to 180 s. All images were first bias subtracted and then pair-wise subtracted to give the final image. All resultant images were deeper than the 2MASS J-band image for the same field.

SpeX has a 512×512 array InSb camera with a $60'' \times 60''$ FOV and a $0''.12$ pixel scale (Rayner et al. 2003). We used this camera to image candidates during 31 May 2006 UT, 17–18 Aug 2006 UT, 01–02 Sep 2006 UT, 17 Nov 2006 UT, and 08–09 & 20–21 Dec 2006 UT. Conditions for the 31 May 2006 UT run were clear with $1''$ seeing at J-band. Conditions were also clear with $0''.6$ – $0''.7$ seeing at J-band for the 17–18 Aug 2006 UT and 01–02 Sep 2006 UT runs. Conditions for the 17 Nov 2006 run ranged from clear to light cirrus with $1''.0$ seeing at K-band and similar conditions for the 08–09 & 20–21 Dec 2006 UT runs with $0''.5$ – $0''.8$ seeing at K-band. Using the J-band filter, we took 60 sec exposures with a single offset for pair-wise subtraction. In all cases where neighboring stars fell in the camera’s FOV, we were able to verify that the resultant images were deeper than the 2MASS J-band image for the same field. Candidates absent in our two imaging campaigns are listed in Table 2.

2.3. Spectroscopy: IRTF 3.0m/SpeX

Spectroscopic observations were obtained using the IRTF/SpeX spectrograph in low-resolution mode, covering ~ 0.7 – $2.5 \mu\text{m}$ in a single order on the 1024×1024 InSb array.

⁶Located on the summit of Mauna Kea, Hawai’i.

⁷See <http://www.ifa.hawaii.edu/88inch/2.2-meter-technical.htm>

We used the 0.5 slit, resulting in $R \sim 150$, and rotated the slit to the parallactic angle to minimize slit losses. For accurate sky subtraction, we nodded along the slit in ABBA cycles. Exposure times for science targets ranged from 120–180 s to maximize signal-to-noise and to minimize temporal variations of OH airglow, which can leave a forest of residual lines for long exposures (see Figures 1, 2, & 3 of Ramsay et al. 1992).

We obtained spectroscopic observations for a total of 20 science targets, 2 T dwarf standards, and 20 calibrator A0 V stars between 08 Apr 2006 UT and 21 Dec 2006 UT. We list a log of our observations in Table 3. All nights were clear or had light cirrus. All calibrator A0 stars were observed either immediately before or after the science target with a differential airmass less than 0.10 for accurate flux calibration. After observing the calibrator stars, we immediately took internal flat-field and argon arc lamps for instrumental calibration. We employed standard reduction techniques using the Spextool package version 3.2 (Cushing et al. 2004; Vacca et al. 2003).

3. Analysis

3.1. M Dwarfs

Near-infrared spectroscopy of candidates confirmed via second-epoch imaging (see §2.2) reveals nine of them as M dwarfs. To classify these spectra, we compared their overall morphology, particularly the strength of their H₂O absorptions at 1.30–1.51 and 1.75–2.05 μm , to a set of known M dwarfs: Gl 229A (M1), Gl 411 (M2), Gl 388 (M3), Gl 213 (M4), Gl 51 (M5), Gl 406 (M6), vB8 (M7), vB10 (M8), LHS 2924 (M9), and BRI 0021–0214 (M9.5) (Cushing et al. 2005). We list the spectral types (M3–M7) of these nine M dwarfs in Table 3 and estimate our accuracy as ± 1 subtype, except for those types denoted with a colon due to spectra with poor signal-to-noise. None of these 9 M dwarf spectra differ markedly from our comparison M dwarfs, suggesting that the unusual near-infrared colors of these M dwarfs shown in Figure 1 are due to large photometric errors instead of spectroscopic peculiarities.

3.2. T Dwarfs

3.2.1. Classification & Kinematics

In Figure 3, we show finder charts for all 11 new T dwarfs constructed from 2MASS All-Sky Release Survey⁸ J-band images. We classified these T dwarfs by comparing their overall spectral morphologies to near-infrared T dwarf primary standards (see Figure 4) defined by Burgasser et al. (2006a): SDSS J120747.17+024424.8 (T0 std), SDSSp J083717.22–000018.3 (T1 std), SDSSp J125453.90–012247.4 (T2 std), 2MASS J12095613–1004008 (T3 std), 2MASSI J2254188+312349 (T4 std), 2MASS J15031961+2525196 (T5 std), SDSSp J162414.37+002915.6 (T6 std), 2MASSI J0727182+171001 (T7 std), and 2MASSI J0415195–093506 (T8 std). These were also observed with IRTF/SpeX using the 0".5 slit, so they have identical resolution ($R \sim 150$) to our spectra (Burgasser et al. 2006a, and this paper). We calculated near-infrared H₂O and CH₄ spectral indices defined in Burgasser et al. (2006a) for the 11 new T dwarfs (see Table 5). The indirect spectral types (calculated by comparing each index measurement to that of each standard and finding the nearest subtype or half subtype match) are in excellent agreement (≤ 0.5 subtypes) with our direct spectral classification except for 2MASS 0729–39, which has two indices that are classified as $> T8$ and are not included in the mean indirect spectral type.

We find a spectral type range of T2 to T8 and a wide range in color of $-0.6 \lesssim J-K_s \lesssim 1.5$. We were able to identify early-type T dwarfs in 2MASS because we did not rely on near-infrared color selections in our proper motion search. With the exception of 2MASS 1324+63 (T2:pec) and 2MASS 0729–39 (T8pec), these T dwarfs show CH₄ and H₂O absorption strengths throughout the near-infrared regime consistent with standards of similar spectral types (see Figure 4). In Figure 5, we show the near-infrared (J, H, K_s) colors along with optical (i, z) colors, when available, of these 11 T dwarfs in comparison to all known T dwarfs with individual magnitude errors of less than 0.3 mag.

The near-infrared colors of these new T dwarfs span a broad range, but generally track with the trend in color as a function of spectral type. While 2MASS 1324+63 lies along the redder edge of the dispersal relative to objects of similar spectral type and 2MASS 0729-39 lies along the bluer edge relative to objects of similar spectral type, they are both within one sigma of their own photometric errors from other sources in the dispersion.

Although the bottom panel of far optical minus near-infrared colors has very few sources, 2MASS 1324+63 is indistinct from the scatter of other T2 dwarfs. On the other hand, 2MASS

⁸See <http://irsa.ipac.caltech.edu/Missions/2mass.html>.

1106+27 is the only T2.5 dwarf with a measured i-band color in SDSS but is distinctly ($> 1\sigma$) bluer than all T2 dwarfs and is the bluest T2.5 dwarf in z–J. Although 2MASS 1106+27 is the second brightest T dwarf in SDSS ($z=17.70\pm 0.03$, see Table 4), it was not found in previous searches of SDSS for T dwarfs because the photometry for a nearby faint source was registered instead. To get the SDSS colors for this object, we had to use the Navigate Visual Tool⁹ to find 2MASS 1106+27. We used the Explore radio button and recorded the parameters of this object, which we fed to an SQL query, requesting the psf magnitudes (see Table 4). The i and z magnitudes of 2MASS 1324+63 and 2MASS 1615+13, we obtained from the SDSS Catalog in a standard fashion, requesting the ‘psf_mags’ and ‘psf_magerrs’ (see Table 4).

Spectrophotometric distance estimates were calculated using the spectral types derived above and the Liu et al. (2006) spectral type vs. magnitude relation (excluding known binaries) and are given along with other spectrophotometric properties in Table 4. These distances range from ~ 8.4 –29.0 pc. For the three early-type T dwarfs from the 2MASS proper motion survey, we were able to calculate proper motions and position angles from the multi-epoch data (see Table 6 for kinematic properties). We were also able to do the same for 2MASS 1615+13, which was detected in z-band in the SDSS Catalog. The proper motions along with the distance estimates yielded tangential velocity estimates of ~ 36 –66 km s^{-1} for these four objects, which are near or exceeding the median $V_{tan} = 39.0 \text{ km s}^{-1}$ for T dwarfs found by Vrba et al. (2004). The tangential velocities of these four T dwarfs are nearly twice that of the median tangential velocities of L dwarfs ($V_{tan} = 24.5 \text{ km s}^{-1}$, Vrba et al. 2004). Our proper motion sample is biased towards these higher velocity objects; i.e., at a distance of 20 pc, we would only detect objects with $V_{tan} \gtrsim 4.74 \times 0''.4 \text{ yr}^{-1} \times 20 \text{ pc} = 38 \text{ km s}^{-1}$. We use $0''.4 \text{ yr}^{-1}$ in this estimate since $0''.4$ is the motion floor for the survey and the mean epoch difference is near 1 yr.

3.3. Spectroscopically Peculiar Sources

Two of the T dwarfs identified in this study have spectral properties that are somewhat unusual compared to the spectral standards. We discuss these peculiar sources in detail.

⁹See <http://cas.sdss.org/astrodr5/en/tools/chart/navi.asp>.

3.3.1. 2MASS 1324+63 (T2:pec)

While the spectrum of 2MASS 1324+63 has an overall spectral morphology similar to the T2 standard, particularly from the red optical to the blue slope of the H-band peak (1.5 μm), at longer wavelengths it is considerably more red, with weaker CH_4 absorption at 1.6 μm and a brighter K-band peak (2.1 μm). This motivates our classification of this source as peculiar. There are a handful of peculiar T dwarfs known, some of which are known to be binary (e.g., 2MASS J05185995–2828372; Cruz et al. 2004) or suspected to be affected by gravity effects (e.g., 2MASS J0937347+293142; Burgasser et al. 2002, 2006b; Knapp et al. 2004). We consider both of these possibilities for 2MASS 1324+63.

To examine the binary hypothesis, we constructed a suite of synthetic binaries from L8–T8 spectral templates with equivalent SpeX prism spectra¹⁰. Our technique is similar to that used in Burgasser et al. (2005b, 2006c) and Reid et al. (2006). Our spectral templates include the primary near-infrared T dwarf spectral standards defined by Burgasser et al. (2006a) and the L dwarfs 2MASSW J1632291+190441 (L8, Kirkpatrick et al. 1999) and 2MASSW J0310599+164816 (L9, Kirkpatrick et al. 2000). We augmented the SpeX spectra from Burgasser et al. (2006a) with new spectra for SDSS J120747.17+024424.8 (T0; Hawley et al. 2002) and SDSSp J083717.22–000018.3 (T1; Leggett et al. 2000). Most of these sources are unresolved in high angular resolution imaging (Burgasser et al. 2006c,a and references therein), with the exception of 2MASS 0310+16, which is a near equal-brightness binary (Stumpf et al. 2005). The L9, T0, T3, and T7 templates have yet to be imaged at high angular resolution.

Integrated light spectra for artificial binaries were constructed by first absolutely flux calibrating the A+B spectral components. We computed a correction factor to scale the spectrum of each component such that it had the appropriate absolute J-band magnitude given by its spectral type. The correction factor is given by,

$$C_J = 10^{-0.4 M_J} \frac{\int \lambda f_\lambda^{Vega}(\lambda) T_J(\lambda) d\lambda}{\int \lambda f_\lambda^{obs}(\lambda) T_J(\lambda) d\lambda}$$

where both the J-band Vega spectrum¹¹, f_λ^{Vega} , and the 2MASS J-band transmission profile¹², $T_J(\lambda)$, have been interpolated onto the wavescale of each observed component. The absolute J-band magnitude, M_J , was computed from the Liu et al. (2006) spectral type vs absolute magnitude relation, excluding known binaries. We calculated and multiplied this

¹⁰Synthetic spectra available upon request.

¹¹Downloadable from Sandy Leggett’s site – <ftp://ftp.jach.hawaii.edu/pub/ukirt/skl/filters/vega.obs>.

¹²See http://spider.ipac.caltech.edu/staff/waw/2mass/opt_cal/jrsr.tbl.html.

correction factor for both A+B components. Then we interpolated the wavelength scale of the B component onto the wavelength scale of the A component and added the two fluxes for the combined synthetic spectrum. For quantitative reference, we calculated H₂O and CH₄ spectral indices for the entire suite (see col. 2–6, Table 7) but classify the synthetic spectra on overall morphology in comparison with spectral standards (see col. 9 – Direct, Table 7). The spectral type of each synthetic combination computed by the indices is shown in col. 10 of Table 7 (Ind 1). These indices are shown graphically in Figure 6 for the NIR synthetic spectra, NIR T dwarf standards, and the 11 new T dwarfs.

The synthetic binary spectra were compared to the spectrum of 2MASS 1324+63 visually. The four closest matches are shown in Figure 7. The best two matches are L9+T2 [T0.5] and L8+T5 [T2:]. The L9+T2 synthetic combination, while providing a fairly good match throughout most of H- and K_s-bands and having comparable H₂O absorption strength from 1.75–2.05 μm, has weaker H₂O absorption from 1.3–1.5 μm, a weaker Y-band (~0.93–1.15 μm; Hillenbrand et al. 2002) slope, and weaker CH₄ and H₂O absorption from ~1.1–1.2 μm. The L8+T5 synthetic combination, conversely, provides a good match in Y- and J-bands but has overly strong absorption in H- and K-bands, which are primarily shaped by CH₄ absorption and CIA H₂. While none of these matches are ideal, it should be noted that similar analysis for the resolved binary DENIS-P J225210.73–173013.4 also fails to provide a perfect fit, even though the source is known to be a binary (Reid et al. 2006). So unresolved multiplicity may nevertheless play a significant role.

Another possibility is that 2MASS 1324+63 is a young T dwarf (< 300 Myr), implying a lower mass, larger radius, and hence lower surface gravity (low pressure photosphere). One of the primary spectral shapers in K-band and, to a lesser extent, H-band, is CIA H₂. In a low pressure atmosphere, the contribution of CIA H₂ would decrease and the spectrum would become redder (J–K would increase). This effect has been noted for young L dwarfs (Kirkpatrick et al. 2006, Kirkpatrick et al. in prep). 2MASS 1324+63 could also have a dustier photosphere than typical T2 dwarfs, possibly caused by a lower gravity environment retarding the precipitation of dust. To date, the youngest spectroscopically confirmed T dwarf¹³ is HN Peg B (Luhman et al. 2007), a T2.5 companion to HN Peg A (a G0 V star estimated to be ~300 Myr old). After ~300 Myr, brown dwarf radii contract very little, differing by only ~20% in radius from their much older 3 Gyr counterparts (Burrows et al. 1997). While this relatively young object is less massive than a 3 Gyr T2.5 dwarf, HN Peg B shows no spectroscopic deviations from a typical field T2.5 dwarf (See Figure 8 and Luhman

¹³A candidate very low mass T dwarf in the ~1 Myr Orion cluster, S Ori 70, has been proposed by Zapatero Osorio et al. (2002) and Martín & Osorio (2003). However, this source remains controversial (Burgasser et al. 2004a).

et al. 2007).

2MASS 1324+63 is located in a region of sky completely unoccupied by any currently known young moving group. It could be a member of an unidentified young moving group or it could be older (> 100 Myr) than most moving groups (either a cast-off or from a dispersed group). Its tangential velocity ($V_{tan} = 45 \text{ km s}^{-1}$) seemingly contradicts this, suggesting that it is of comparable age to older field T dwarfs.

3.3.2. 2MASS 0729–39 (*T8pec*)

This object is one of four spectroscopically classified T8 dwarfs, the latest spectral type for T dwarfs currently known. While the peculiarities of 2MASS 0729–39 are not as evident as those for 2MASS 1324+63, they are certainly noticeable and worth further exploration here. This source is peculiar because it has some excess flux in the Y-band peak while the J-band peak, the H₂O and CH₄ absorption from $\sim 1.1\text{--}1.2 \mu\text{m}$, and the H₂O absorption from $1.3\text{--}1.5 \mu\text{m}$ matches well to the T8 standard. There is also reduced flux in the H-band and K-band peaks compared to the T8 standard.

These peculiarities are indicative of a higher pressure photosphere, increasing K I wing absorption (causing slightly increased Y-band flux) and CIA H₂ absorption (causing depressed H- and K-band flux). Such features were previously noted for the high surface gravity and metal poor dwarf 2MASS 0937+29 (See Figure 2 of Burgasser et al. 2006b). 2MASS 0729–39 may be a similarly relatively old and/or slightly metal-poor T dwarf.

3.4. Temperatures & Gravities

To examine the properties of our latest-type T dwarfs in further detail, we made use of the semi-empirical spectral index technique of Burgasser et al. (2006b) to estimate T_{eff} and $\log g$. In brief, this method involves the comparison of H₂O and color spectral ratios measured on the spectrum of a late-type T dwarf to the same ratios measured on theoretical condensate-free spectral models from Allard et al. (2001) and Burrows et al. (2006). The latter are calibrated to reproduce the measured indices for the near infrared SpeX prism spectrum of Gliese 570D (Burgasser et al. 2000a), which has parameters of $T_{eff} = 782\text{--}821 \text{ K}$, $\log g = 4.95\text{--}5.23$ and $[\text{Fe}/\text{H}] = 0.09 \pm 0.04$, based on empirical measurements and evolutionary models (Geballe et al. 2001; Saumon et al. 2006). The H₂O and color ratios are separately sensitive to T_{eff} and $\log g$ (for a given metallicity), and thus break the degeneracy between these parameters, which can then be used to infer mass and age with evolutionary

models. As condensate-free spectral models generally provide poor fits for $T_{eff} \gtrsim 1200$ K, our analysis is generally confined to sources $\gtrsim T5$ (Golimowski et al. 2004). See Burgasser (2007) and Liebert & Burgasser (2007) for examples of this spectral technique in application.

We were able to derive constraints for T_{eff} and $\log g$ for five of the new T dwarfs in our sample using the H_2O -J and K/H ratios (the latter defined in Burgasser et al. 2006b). Figure 9 illustrates the fits for these sources, and Table 8 lists their estimated T_{eff} and $\log g$ ranges assuming an uncertainty of 10% in the spectral ratio measurement. Note that additional systematic uncertainties of order 50 K and 0.2 dex should be included when interpreting these values. T_{eff} values are consistent with trends from parallax samples (Golimowski et al. 2004; Vrba et al. 2004), and show the expected decline in T_{eff} with later spectral type. Note that the peculiar T8, 2MASS 0729–39 has a relatively large surface gravity, consistent with our interpretation of this source in § 3.5.2. 2MASS 1007–45, on the other hand, has a relatively low surface gravity, which is consistent with its brighter K-band flux peak as seen in Figure 3 relative to the T5 standard. Subsolar and supersolar metallicities can also reproduce these effects, respectively (Burgasser et al. 2006b; Burgasser 2007; Liu et al. 2007; Saumon et al. 2007).

Using the solar metallicity evolutionary models of Burrows et al. (2001), we estimated masses and ages for these five sources; ranges (without including systematic uncertainties) are given in Table 8. As expected, low (high) surface gravities result in low (high) mass and age estimates. Since metallicity effects can mimic surface gravity effects on the K-band (in both cases modulating the relative opacity of H_2), care should be taken in interpreting these values.

4. Discussion - The Solar Neighborhood

To place our discoveries in context and to review the current state of high-resolution imaging for the nearest T dwarfs, we have constructed an up-to-date census of T dwarfs in the Solar Neighborhood (< 25 pc). This list was constructed from the L & T dwarf compendium maintained by Kirkpatrick, Gelino, & Burgasser¹⁴. We computed spectrophotometric distance estimates for the entire list of T dwarfs, using the M_J vs near-infrared (NIR) SpT relation derived by Liu et al. (2006) (excluding known binaries). Those T dwarfs with trigonometric parallaxes have their distance estimates superseded by these measurements. For T dwarfs known to be binaries but without parallaxes, we have placed lower limits on their spectrophotometric distance estimate. Within 25 pc, this list includes a total

¹⁴See <http://dwarfarchives.org>.

of 72 T dwarfs, including 9 new additions reported here (see Table 9). These new additions represent an $\sim 14\%$ increase in the 25 pc census of T dwarfs. Only 1 T dwarf from the compendium meeting these criteria was excluded from this list – 2MASS J11263991–5003550 (NIR T0, Folkes et al. 2007), which Burgasser et al. in prep, demonstrate has a mid-type L dwarf optical spectral morphology.

Within 10 pc, there are currently 14 known T dwarfs, one of which, 2MASS 0729–39 (the 8th closest T dwarf to the sun at 8.4 pc), is reported here. Of these 14 T dwarfs, 5 are companions to more massive stars. To date, over half of these T dwarfs have been followed-up with high-resolution imaging, with one revealed as a tight binary - the nearest T dwarf, ϵ Indi Bab (Scholz et al. 2003; McCaughrean et al. 2004). This yields a binary fraction of $\sim 13\%$ and a lower limit to the observed space density of 3×10^{-3} T dwarfs per pc^3 for the 10 pc sample. Metchev et al. in prep, performed Monte Carlo simulations, predicting ~ 30 T0–T8 dwarfs within 10 pc (a space density of $7_{-3.0}^{+3.2} \times 10^{-3} \text{ pc}^{-3}$), roughly twice the known population. The inputs for these simulations were based on a critical examination of T dwarf candidates chosen from a cross-correlation of SDSS and 2MASS, which helps to eliminate the 2MASS selection bias for early-T dwarfs and the SDSS selection bias for very late-T dwarfs. This density estimate exceeds both that derived for T5–T8 dwarfs ($4.2 \times 10^{-3} \text{ pc}^{-3}$; Burgasser et al. 2002) and for L dwarfs ($3.8 \times 10^{-3} \text{ pc}^{-3}$; Cruz et al. 2007).

Between 10 and 25 pc, there are currently 59 known T dwarfs, 8 of which we report here. One caveat to this set, is that the distances we assigned to non-parallax sources are biased into this sample if they are binary (i.e., they are really further away, potentially outside 25 pc). The state of high-resolution imaging for this sample is not nearly as complete as for $d < 10$ pc, with only 23 out of the 59 known T dwarfs having follow-up. Of these 23 T dwarfs, 7 have been identified as binaries (Burgasser et al. 2006c and references there-in), yielding a binary fraction of $\sim 30\%$ for this sample. This entire list represents an interesting distance-limited subset of all known T dwarfs, complete follow-up (both high resolution imaging and parallax measurements) of which could greatly bolster binarity statistics and lead to a more complete understanding of brown dwarf formation. Based on the number of known T dwarfs within 10 pc, there should be $\gtrsim 200$ T dwarfs within $10 < d < 25$ pc (Metchev et al. in prep, predict ~ 430), so the current census is highly incomplete.

We also note that, like the prototypes of the L and T spectral classes (GD 165B, Becklin & Zuckerman 1988 and Gl 229B, Nakajima et al. 1995; Oppenheimer et al. 1995, respectively), which are both companions, the prototype of the Y spectral class (hypothetical dwarfs cooler than type T, Kirkpatrick et al. 1999) could first be identified as a companion to one of these T dwarfs. This should be ample motivation for the brown dwarf community to continue high angular resolution imaging of our nearest cool neighbors.

5. Conclusions

We have reported on the discovery of 11 new T dwarfs found during the course of two surveys using the 2MASS database. Using low-resolution prism spectroscopy ($R \sim 150$) on IRTF/SpeX, we have classified these T dwarfs in the near-infrared from T2–T8. All of these T dwarfs are nearby, with spectrophotometric distance estimates of ~ 8.4 – 29.0 pc. One of these T dwarfs, 2MASS J13243559+6358284, we type as T2:pec and postulate that its spectroscopic peculiarities are the result of reduced collision induced absorption by H_2 , indicative of it being a young object (< 300 Myr), or that it is an L/T transition binary. To provide models for suspected or known binaries, we constructed a suite of synthetic spectra and computed their H_2O and CH_4 indices. We have also reviewed the state of high resolution follow-up of T dwarfs in the Solar Neighborhood with $d < 25$ pc and make the case for completing follow-up of this sample to improve the poorly sampled binary statistics throughout the T spectral class for this distance-limited set.

6. Acknowledgments

DLL thanks J. Rayner for advising her for part of this project and for a careful read of the manuscript. We would like to thank J. Kartaltepe and Y. Kakazu for imaging several of our targets with the UH 2.2m/ULBCAM and for teaching DLL how to use the instrument. We thank S. Metchev for helping us with the SDSS Catalog, Mike Cushing for useful discussions, and Kevin Luhman for kindly providing the spectrum of HN Peg B. We would also like to thank our telescope operators on IRTF: D. Griep & B. Golisch. This paper uses data from the IRTF Spectral Library (<http://irtfweb.ifa.hawaii.edu/~spex/spexlibrary/IRTFlibrary.html>) and from <http://DwarfArchives.org>. This publication also makes use of data products from the Two Micron All Sky Survey (2MASS), which is a joint project of the University of Massachusetts and the Infrared Processing and Analysis Center/California Institute of Technology, funded by the National Aeronautics and Space Administration and the National Science Foundation. DLL was a guest user of the Canadian Astronomy Data Centre, which is operated by the Herzberg Institute of Astrophysics, National Research Council of Canada. This research has also made use of the NASA/IPAC Infrared Science Archive (IRSA), which is operated by the Jet Propulsion Laboratory, California Institute of Technology, under contract with the National Aeronautics and Space Administration. As all spectroscopic and imaging follow-up data were obtained from the summit of Mauna Kea, the authors wish to recognize and acknowledge the very significant cultural role and reverence that this mountaintop has always had within the indigenous Hawaiian community. We are most fortunate to have the opportunity to conduct observations on the summit.

REFERENCES

- Allard, F., Hauschildt, P. H., Alexander, D. R., Tamanai, A., & Schweitzer, A. 2001, *ApJ*, 556, 357
- Artigau, É., Doyon, R., Lafrenière, D., Nadeau, D., Robert, J., & Albert, L. 2006, *ApJ*, 651, L57
- Becklin, E. E., & Zuckerman, B. 1988, *Nature*, 336, 656
- Biller, B. A., Kasper, M., Close, L. M., Brandner, W., & Kellner, S. 2006, *ApJ*, 641, L141
- Borysow, A., Jorgensen, U. G., & Zheng, C. 1997, *A&A*, 324, 185
- Burgasser, A. J. 2007, *ArXiv Astrophysics e-prints*, arXiv:astro-ph/0701793
- Burgasser, A. J., Kirkpatrick, J. D., Cruz, K. L., Reid, I. N., Leggett, S. K., Liebert, J., Burrows, A., & Brown, M. E. 2006, *ApJS*, 166, 585
- Burgasser, A. J., Burrows, A., & Kirkpatrick, J. D. 2006, *ApJ*, 639, 1095
- Burgasser, A. J., Geballe, T. R., Leggett, S. K., Kirkpatrick, J. D., & Golimowski, D. A. 2006, *ApJ*, 637, 1067
- Burgasser, A. J., Reid, I. N., Leggett, S. K., Kirkpatrick, J. D., Liebert, J., & Burrows, A. 2005, *ApJ*, 634, L177
- Burgasser, A. J., Kirkpatrick, J. D., & Lowrance, P. J. 2005, *AJ*, 129, 2849
- Burgasser, A. J., McElwain, M. W., Kirkpatrick, J. D., Cruz, K. L., Tinney, C. G., & Reid, I. N. 2004, *AJ*, 127, 2856
- Burgasser, A. J., Kirkpatrick, J. D., McGovern, M. R., McLean, I. S., Prato, L., & Reid, I. N. 2004, *ApJ*, 604, 827
- Burgasser, A. J., McElwain, M. W., & Kirkpatrick, J. D. 2003, *AJ*, 126, 2487
- Burgasser, A. J., Kirkpatrick, J. D., Reid, I. N., Brown, M. E., Miskay, C. L., & Gizis, J. E. 2003, *ApJ*, 586, 512
- Burgasser, A. J., Kirkpatrick, J. D., McElwain, M. W., Cutri, R. M., Burgasser, A. J., & Skrutskie, M. F. 2003, *AJ*, 125, 850
- Burgasser, A. J., et al. 2002, *ApJ*, 564, 421

- Burgasser, A. J., et al. 2000, *AJ*, 120, 1100
- Burgasser, A. J., et al. 2000, *ApJ*, 531, L57
- Burgasser, A. J., et al. 1999, *ApJ*, 522, L65
- Burrows, A., Sudarsky, D., & Hubeny, I. 2006, *ApJ*, 640, 1063
- Burrows, A., Hubbard, W. B., Lunine, J. I., & Liebert, J. 2001, *Reviews of Modern Physics*, 73, 719
- Burrows, A., et al. 1997, *ApJ*, 491, 856
- Chiu, K., Fan, X., Leggett, S. K., Golimowski, D. A., Zheng, W., Geballe, T. R., Schneider, D. P., & Brinkmann, J. 2006, *AJ*, 131, 2722
- Cruz, K. L., et al. 2007, *AJ*, 133, 439
- Cruz, K. L., Burgasser, A. J., Reid, I. N., & Liebert, J. 2004, *ApJ*, 604, L61
- Cushing, M. C., Rayner, J. T., & Vacca, W. D. 2005, *ApJ*, 623, 1115
- Cushing, M. C., Vacca, W. D., & Rayner, J. T. 2004, *PASP*, 116, 362
- Ellis, S. C., Tinney, C. G., Burgasser, A. J., Kirkpatrick, J. D., & McElwain, M. W. 2005, *AJ*, 130, 2347
- Folkes, S. L., Pinfield, D. J., Kendall, T. R., & Jones, H. R. A. 2007, *ArXiv Astrophysics e-prints*, arXiv:astro-ph/0703808
- Geballe, T. R., et al. 2002, *ApJ*, 564, 466
- Geballe, T. R., Saumon, D., Leggett, S. K., Knapp, G. R., Marley, M. S., & Lodders, K. 2001, *ApJ*, 556, 373
- Golimowski, D. A., et al. 2004, *AJ*, 127, 3516
- Golimowski, D. A., Burrows, C. J., Kulkarni, S. R., Oppenheimer, B. R., & Brukardt, R. A. 1998, *AJ*, 115, 2579
- Grav, T., & Holman, M. J. 2004, *ApJ*, 605, L141
- Hawley, S. L., et al. 2002, *AJ*, 123, 3409
- Hillenbrand, L. A., Foster, J. B., Persson, S. E., & Matthews, K. 2002, *PASP*, 114, 708

- Kirkpatrick, J. D., Barman, T. S., Burgasser, A. J., McGovern, M. R., McLean, I. S., Tinney, C. G., & Lowrance, P. J. 2006, *ApJ*, 639, 1120
- Kirkpatrick, J. D. 2005, *ARA&A*, 43, 195
- Kirkpatrick, J. D., Neill, R. I., Liebert, J., Gizis, J. E., Burgasser, A. J., Monet, D. G., Dahn, C. C., Nelson, B., & Williams, R. J. 2000, *AJ*, 120, 447
- Kirkpatrick, J. D., Reid, I. N., Liebert, J., Cutri, R. M., Nelson, B., Beichman, C. A., Dahn, C. C., Monet, D. G., Gizis, J. E., & Skrutskie, M. F. 1999, *ApJ*, 519, 802
- Knapp, G. R., et al. 2004, *AJ*, 127, 3553
- Leggett, S. K., et al. 2000, *ApJ*, 536, L35
- Liebert, J., & Burgasser, A. J. 2007, *ApJ*, 655, 522
- Liu, M. C., Leggett, S. K., & Chiu, K. 2007, *ApJ*, 660, 1507
- Liu, M. L., Leggett, S. K., Golimowski, D. A., Chiu, K., Fan, X., Gellae, T. R., Schneider, D. P., & Brinkmann, J. 2006, *ApJ*, 647, 1393
- Luhman, K. L., et al. 2007, *ApJ*, 654, 570
- Martín, E. L., & Osorio, M. R. Z. 2003, *ApJ*, 593, L113
- McCaughrean, M. J., Close, L. M., Scholz, R.-D., Lenzen, R., Biller, B., Brandner, W., Hartung, M., & Lodieu, N. 2004, *A&A*, 413, 1029
- Monet, D. G., et al. 1998, *USNO-A2.0 Catalog*
- Mugrauer, A., Seifahrt, R., & Neuhaeuser, T. M. 2006, *MNRAS*, 373, L31
- Nakajima, T., Oppenheimer, B. R., Kulkarni, S. R., Golimowski, D. A., Matthews, K., & Durrance, S. T. 1995, *Nature*, 378, 463
- Oppenheimer, B. R., Kulkarni, S. R., Matthews, K., & Nakajima, T. 1995, *Science*, 270, 1478
- Ramsay, S. K., Mountain, C. M., & Geballe, T. R. 1992, *MNRAS*, 259, 751
- Rayner, J. T., Toomey, D. W., Onaka, P. M., Denault, A. J., Stahlberger, W. E., Vacca, W. D., Cushing, M. C., & Wang, S. 2003, *PASP*, 115, 362
- Reid, I. N., Lewitus, E., Burgasser, A. J., & Cruz, K. L. 2006, *ApJ*, 639, 1114

- Reid, I. N., Gizis, J. E., Kirkpatrick, J. D., & Koerner, D. W. 2001, *AJ*, 121, 489
- Saumon, D., et al. 2007, *ApJ*, 656, 1136
- Saumon, D., Marley, M. S., Cushing, M. C., Leggett, S. K., Roellig, T. L., Lodders, K., & Freedman, R. S. 2006, *ApJ*, 647, 552
- Saumon, D., Bergeron, P., Lunine, J. I., Hubbard, W. B., & Burrows, A. 1994, *ApJ*, 424, 333
- Scholz, R.-D., McCaughrean, M., J., Lodieu, N., & Kuhlbrodt, B. 2003, *A&A*, 398, 29
- Skrutskie, M. F., et al. 2006, *AJ*, 131, 1163
- Straus, M. A., et al. 1999, *ApJ*, 522, L61
- Stumpf, M. B., Brandner, W., & Henning, T. 2005, *Protostars and Planets V*, 8571
- Tinney, C. G., Burgasser, A. J., Kirkpatrick, J. D., & McElwain, M. W. 2005, *AJ*, 130, 2326
- Tsvetanov, Z. I., et al. 2000, *ApJ*, 531, L61
- Vacca, W. D., Cushing, M. C., & Rayner, J. T. 2003, *PASP*, 115, 389
- Vrba, F. J., Henden, A. A., Luginbuhl, C. B., Guetter, H. H., Munn, J. A. 2004, *AJ*, 127, 2948
- Wilson, J. C., Kirkpatrick, J. D., Gizis, J. E., Skrutskie, M. F., Monet, D. G., Houch, J. R. 2001, *AJ*, 122, 1989
- York, D. G., et al. 2000, *AJ*, 120, 1579
- Zapatero Osorio, M. R., Béjar, V. J. S., Martín, E. L., Rebolo, R., Barrado y Navascués, D., Mundt, R., Eisloffel, J., & Caballero, J. A. 2002, *ApJ*, 578, 536

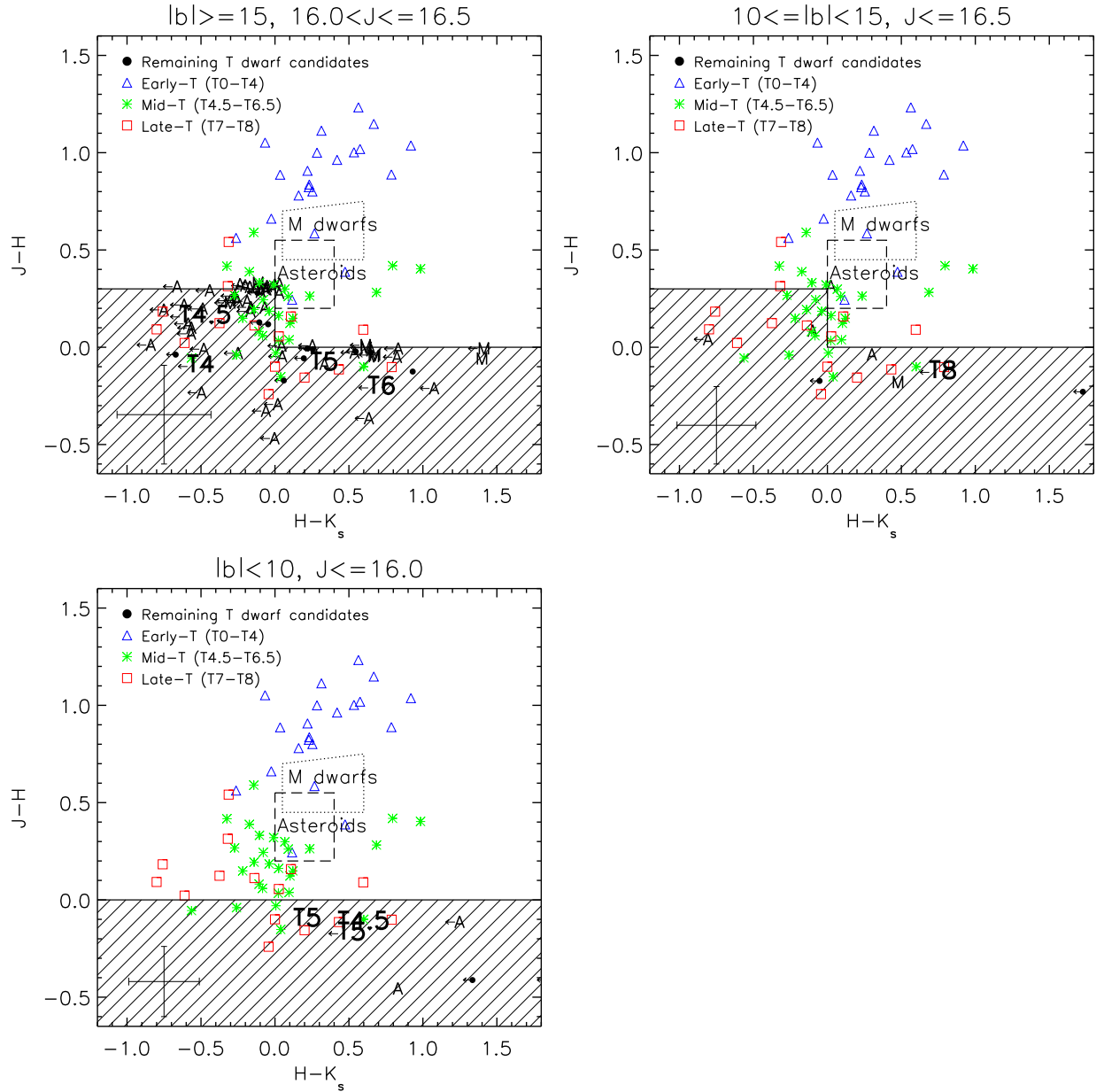


Fig. 1.— Near-infrared color-color plots for the 2MASS photometric search for mid-to-late type T dwarfs broken down by galactic latitude. Color selections are shown by the cross-hatched area. Known T dwarfs are plotted for reference, with early-type T dwarfs represented by blue triangles, mid-type T dwarfs by green asterisks, and late-type T dwarfs by red squares. For reference, the loci of M dwarfs and typical asteroids are outlined (Kirkpatrick et al. 2000; Grav & Holman 2004, respectively). Candidates absent in follow-up imaging are denoted by “A” and spectroscopically confirmed M dwarfs are denoted by “M.” All candidates needing follow-up imaging/spectroscopy are denoted by solid circles and newly identified T dwarfs are denoted by their spectral type. For candidates with null K_s errors, arrows indicate an upper limit on their $H-K_s$ color. Median error bars for all candidates with non-null color errors are shown in the lower left of each plot.

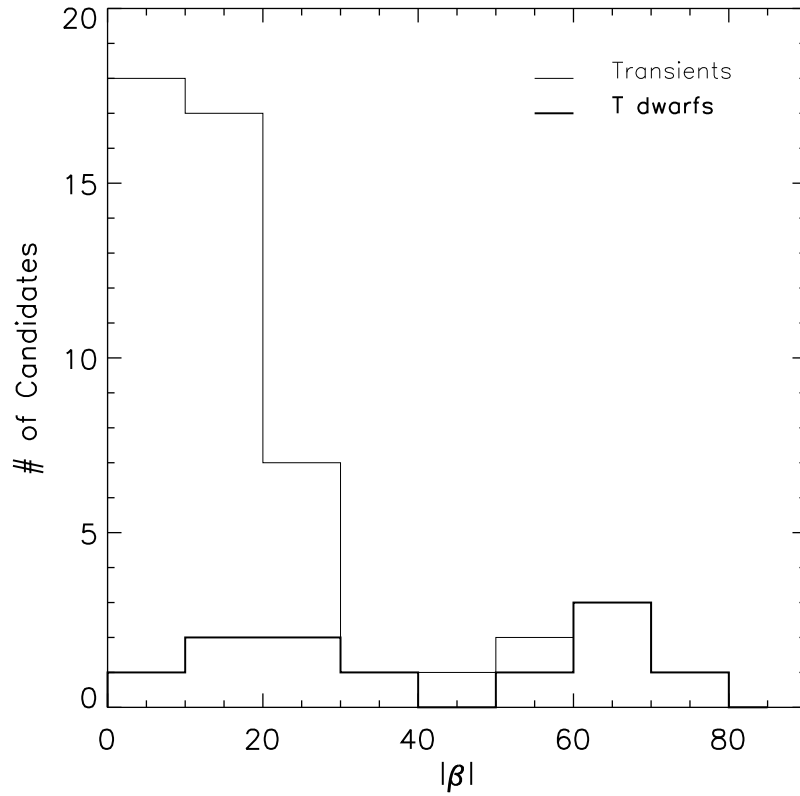
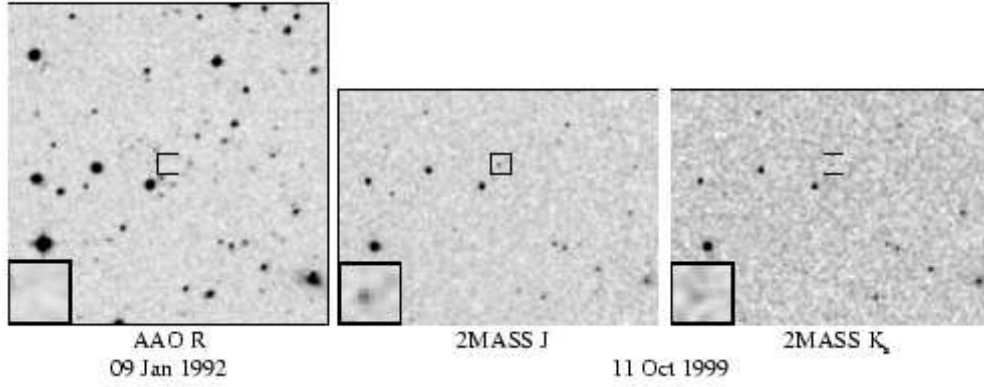
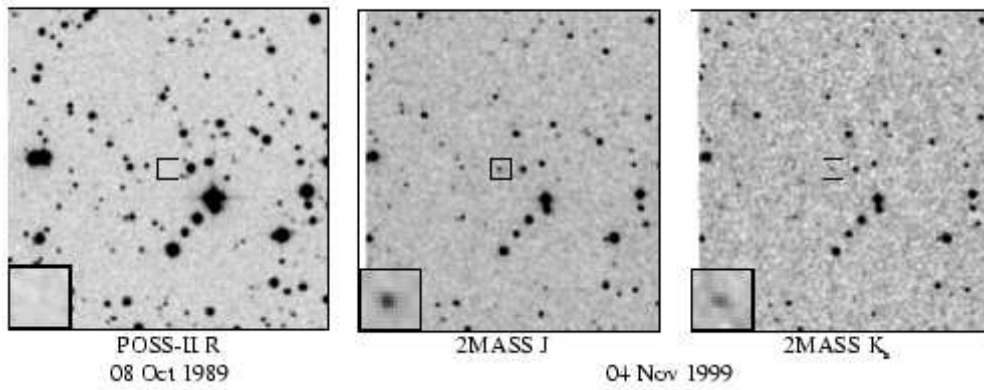


Fig. 2.— A histogram for all 50 transients (light line) and all 8 new T dwarfs and 3 recovered T dwarfs (heavy line), identified in the 2MASS photometric search for mid-to-late type T dwarfs, as a function of ecliptic latitude, $|\beta|$. Note that, while the T dwarfs are distributed nearly evenly across ecliptic latitudes, the vast majority of transients are concentrated near the ecliptic, at $|\beta| \leq 30^\circ$.

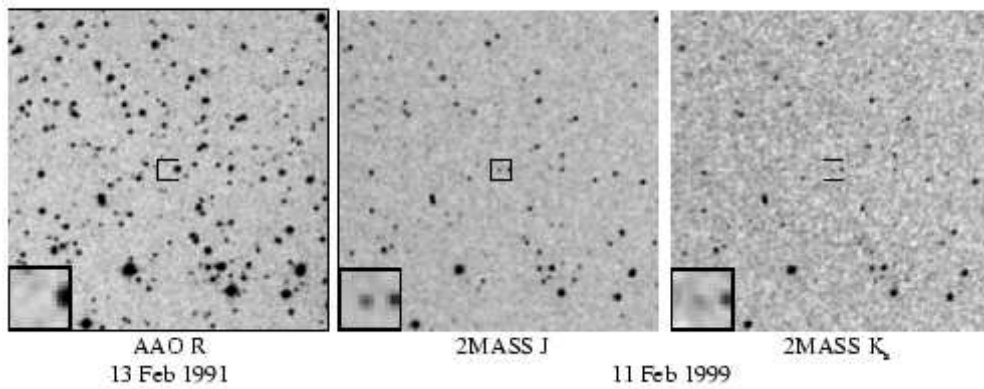
2MASS J05103520-4208140



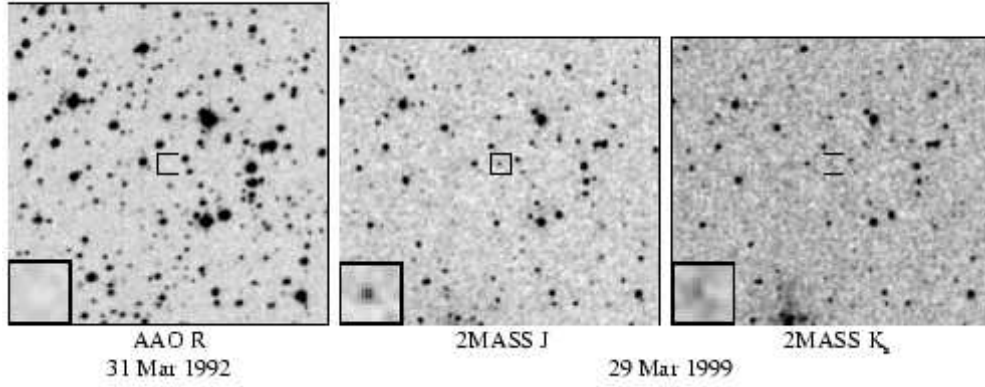
2MASS J06020638+4043588



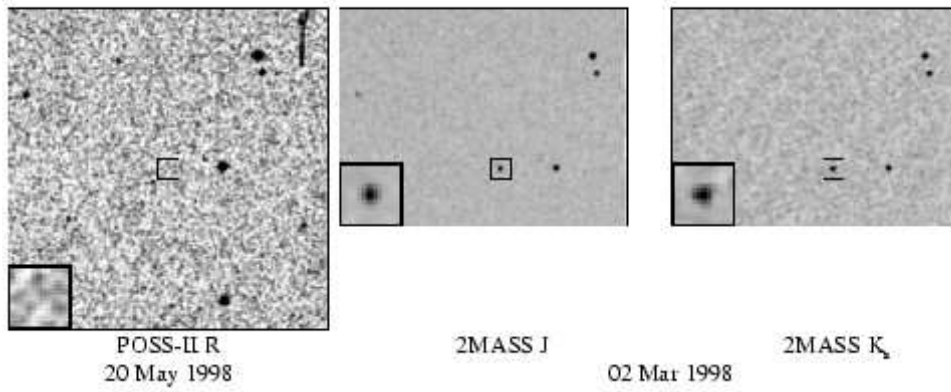
2MASS J07290002-3954043



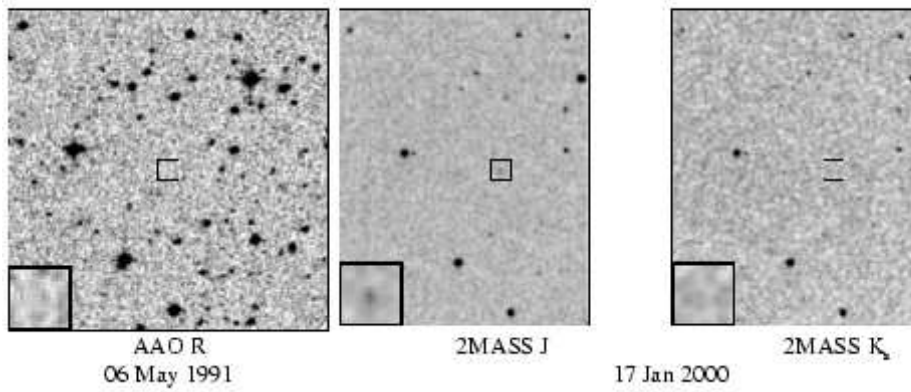
2MASS J10073369-4555147



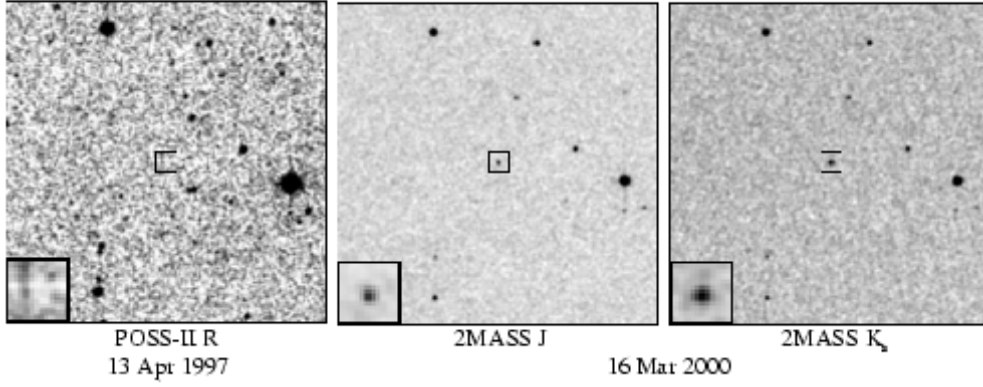
2MASS J11061197+2754225



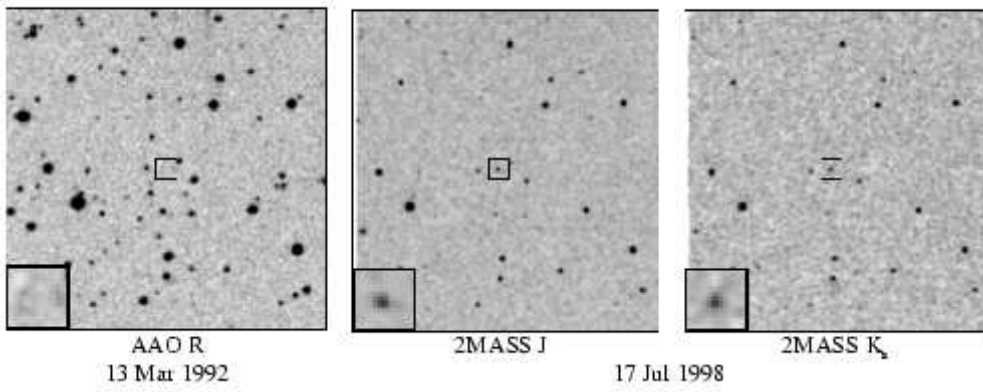
2MASS J12154432-3420591



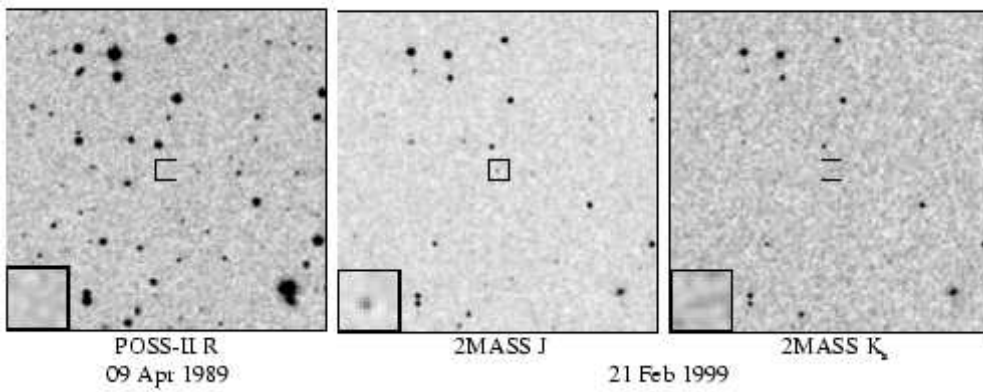
2MASS J13243559+6358284



2MASS J14044941-3159329



2MASS J16150413+1340079



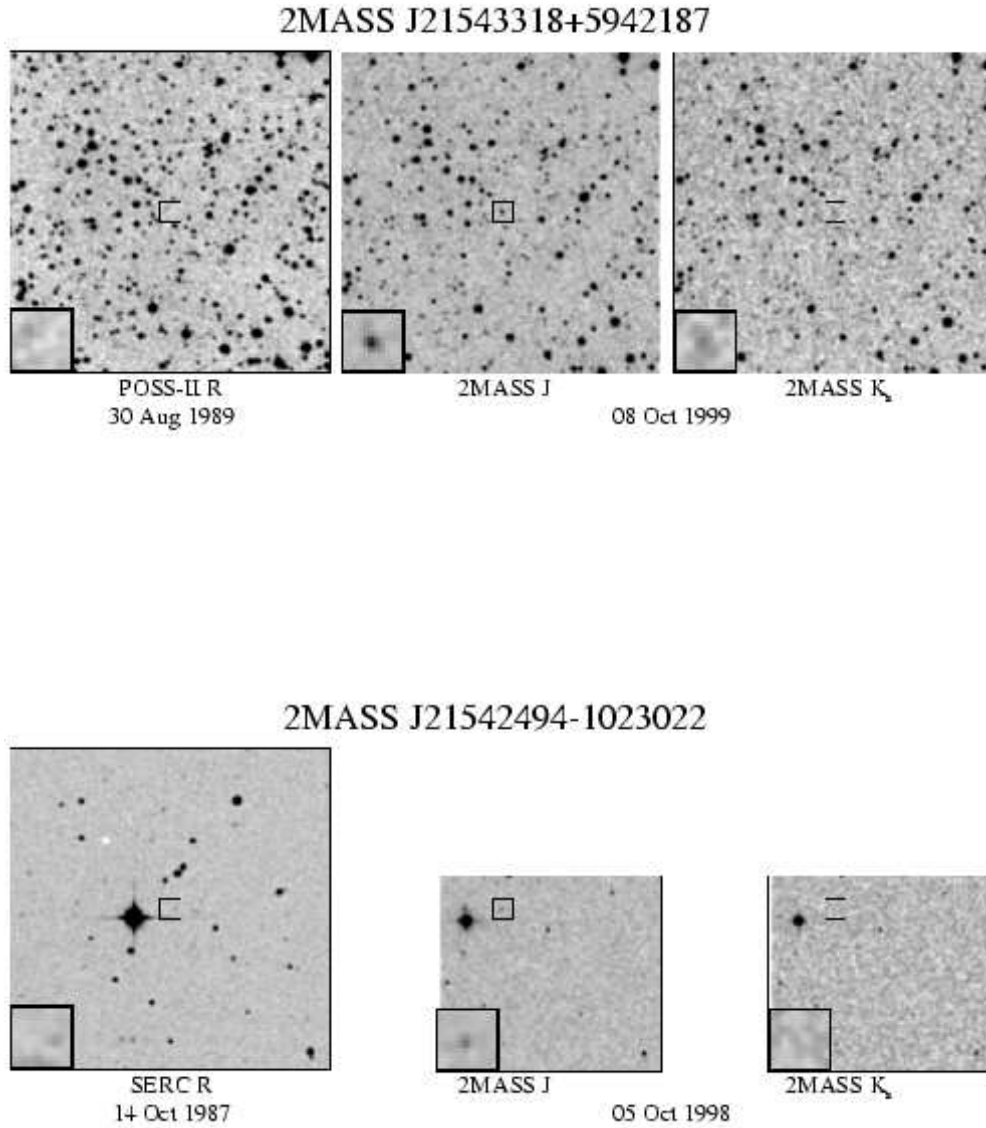


Fig. 3.— Finder charts for the eleven new T dwarfs constructed from DSS II R-band, 2MASS J-band, and 2MASS K_s-band images. Each image is nominally 300'' on a side, although some images near the edge of a scan are smaller in size. Inserts shown on the lower left are 10'' on a side. Epochs (UT) for each image are indicated along with the J2000 coordinates for each object represented by hhmm±ddmm.

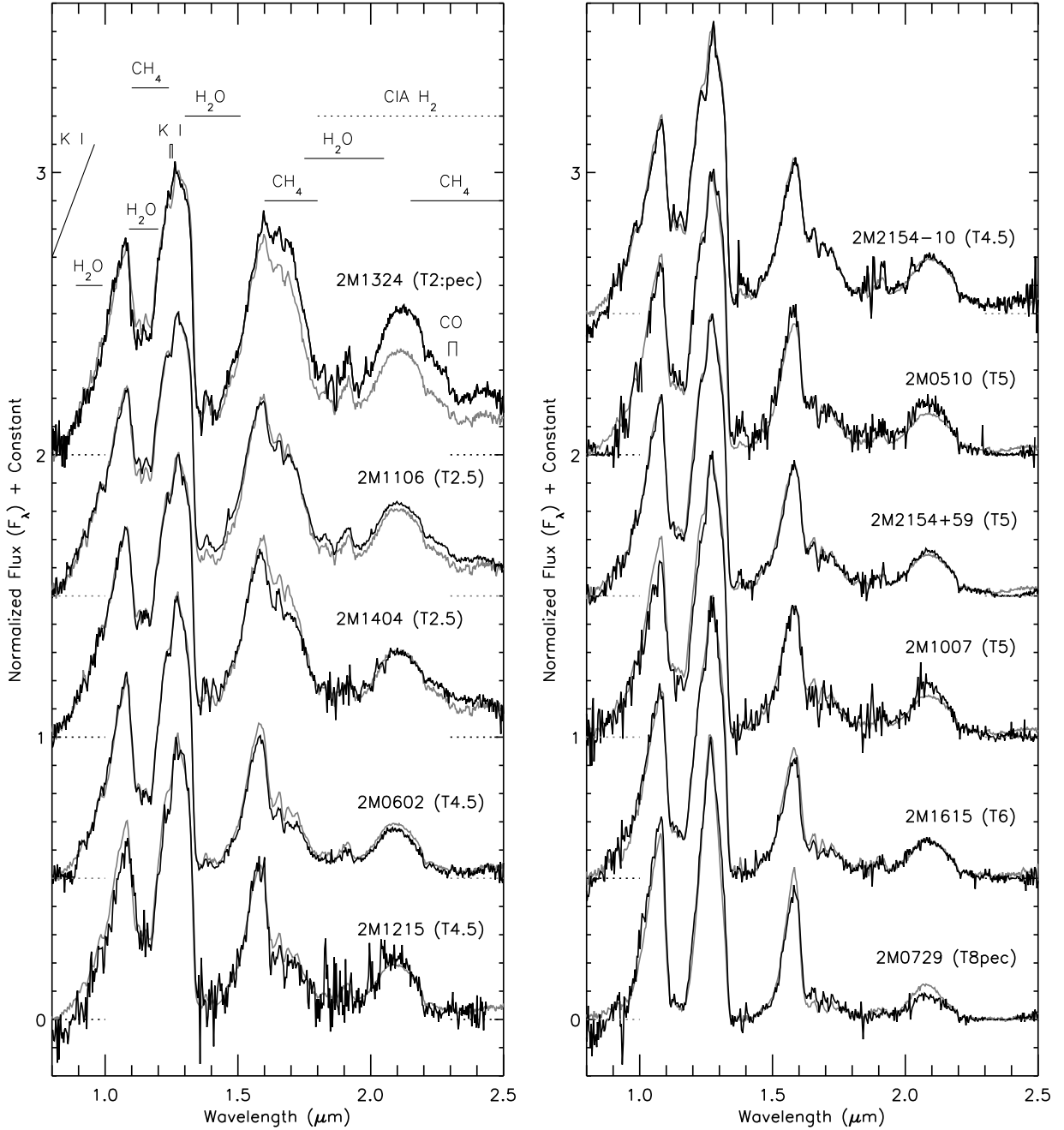


Fig. 4.— IRTF/Spex prism ($R \sim 150$) spectra of the eleven newly discovered T dwarfs (thick black lines) overplotted on their nearest near-infrared spectral type match (thin gray lines). Integer spectral types are the near-infrared primary T dwarf standards defined by Burgasser et al. (2006a). Half subtypes are from the synthetic spectral library (see §3.2). All spectra have been normalized at $1.27 \mu\text{m}$ using a $0.01 \mu\text{m}$ window and are offset by half-integer values (dotted lines show zero levels) for clarity. We have indicated the key atomic and molecular features.

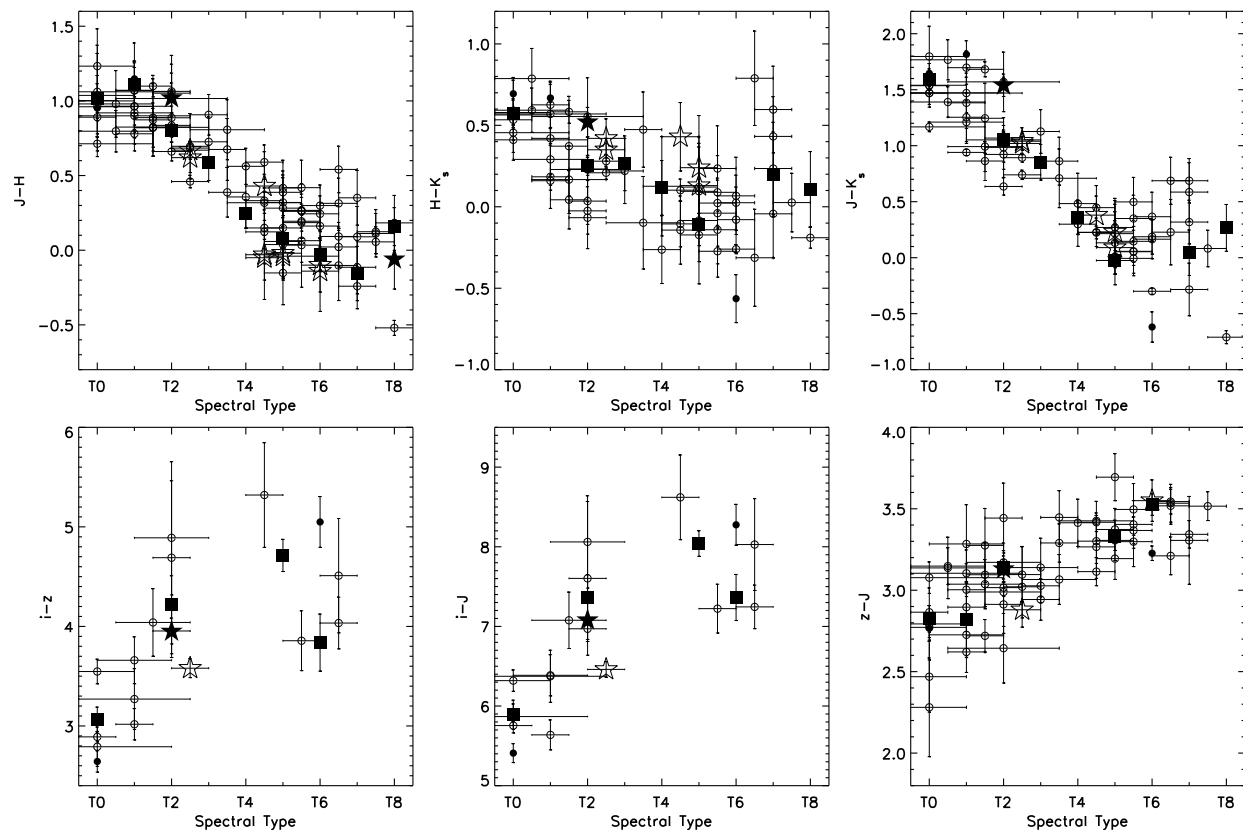


Fig. 5.— Far optical and near-infrared colors of known T dwarfs (open circles), known peculiar T dwarfs (filled circles), T dwarf standards (filled squares), new T dwarfs (open stars), and new peculiar T dwarfs (filled stars) versus near-infrared spectral type. All known T dwarfs shown have magnitude errors of less than 0.3 mag. The i and z magnitudes are from the SDSS (AB) Catalog, and the J , H , and K_s magnitudes are from the 2MASS Catalog.

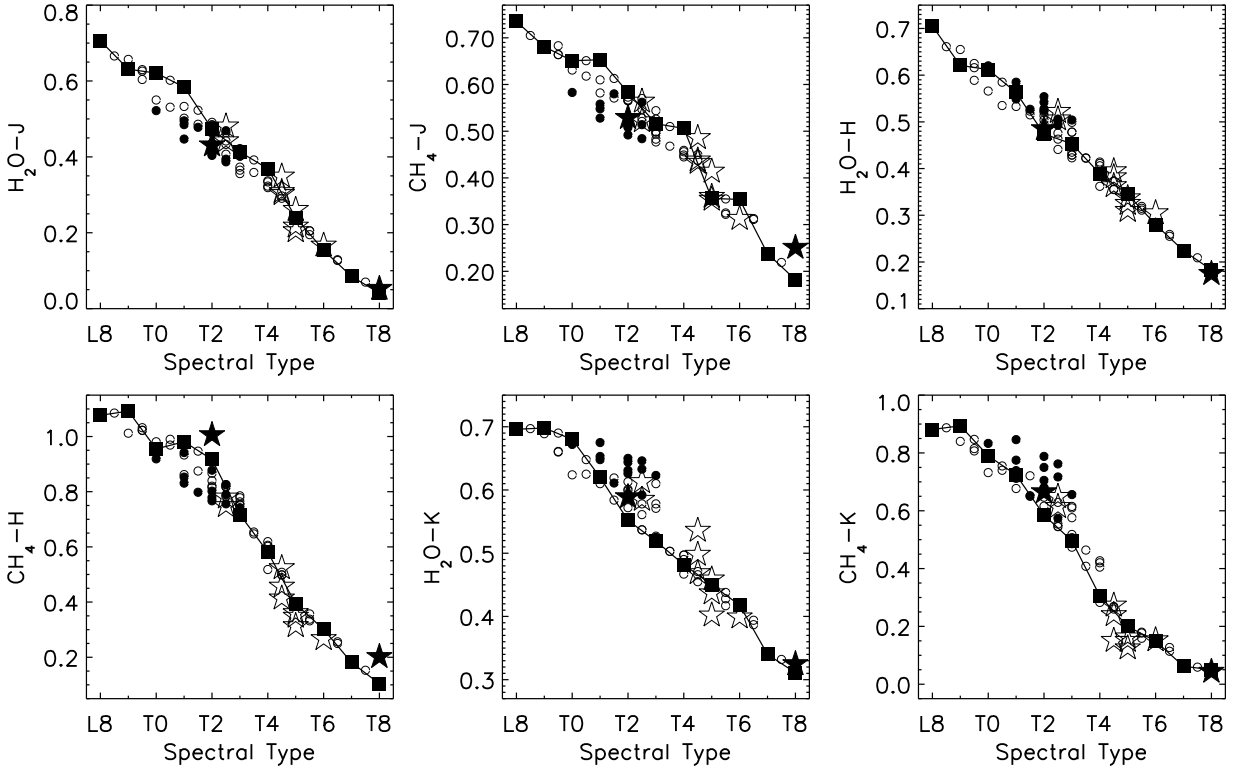


Fig. 6.— Spectral index values of H_2O and CH_4 features versus near-infrared spectral type (determined by direct comparison) as defined by Burgasser et al. (2006a). Solid squares represent the late-type L and T dwarfs we used to create the synthetic spectra, with a solid line connecting them. Synthetic spectra are represented by circles, with peculiar or uncertain types denoted by filled circles. The 11 new T dwarfs reported here are indicated by five-pointed stars, with peculiar sources denoted by filled stars.

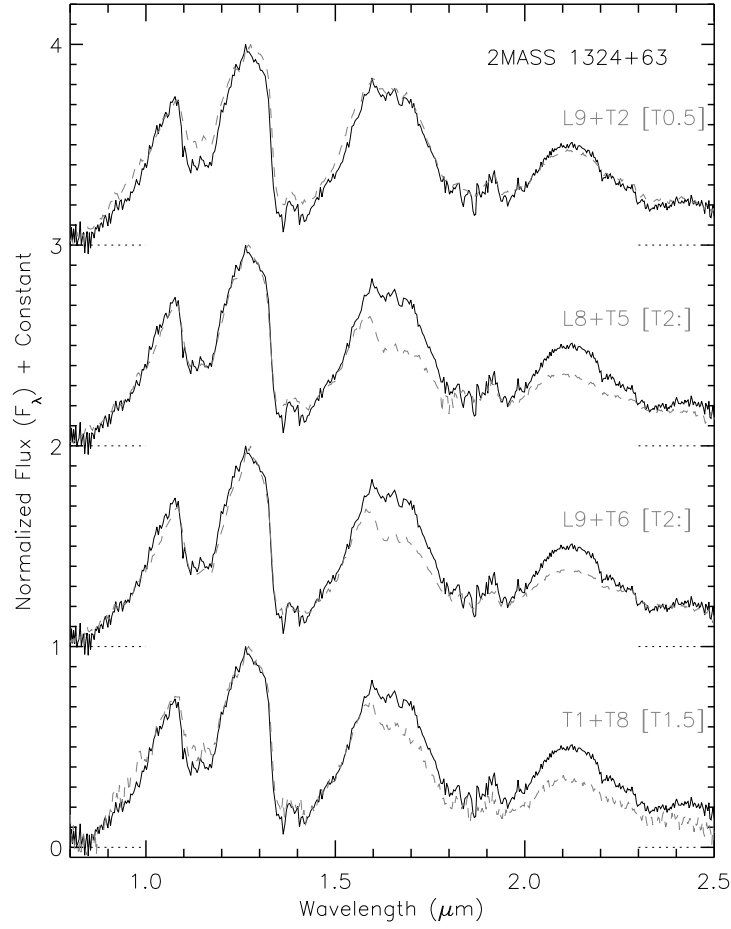


Fig. 7.— Spectral template fitting of 2MASS 1324+63 (black) overplotted with best synthetic spectral fits (gray) determined visually. The A+B components are labeled and the integrated light spectral type (determined by direct comparison) is shown in brackets. All spectra have been normalized at 1.27 μm and are offset by integer units (zero levels are marked by dotted lines) for clarity. Of these four, the best fit is L9+T2 [T0.5].

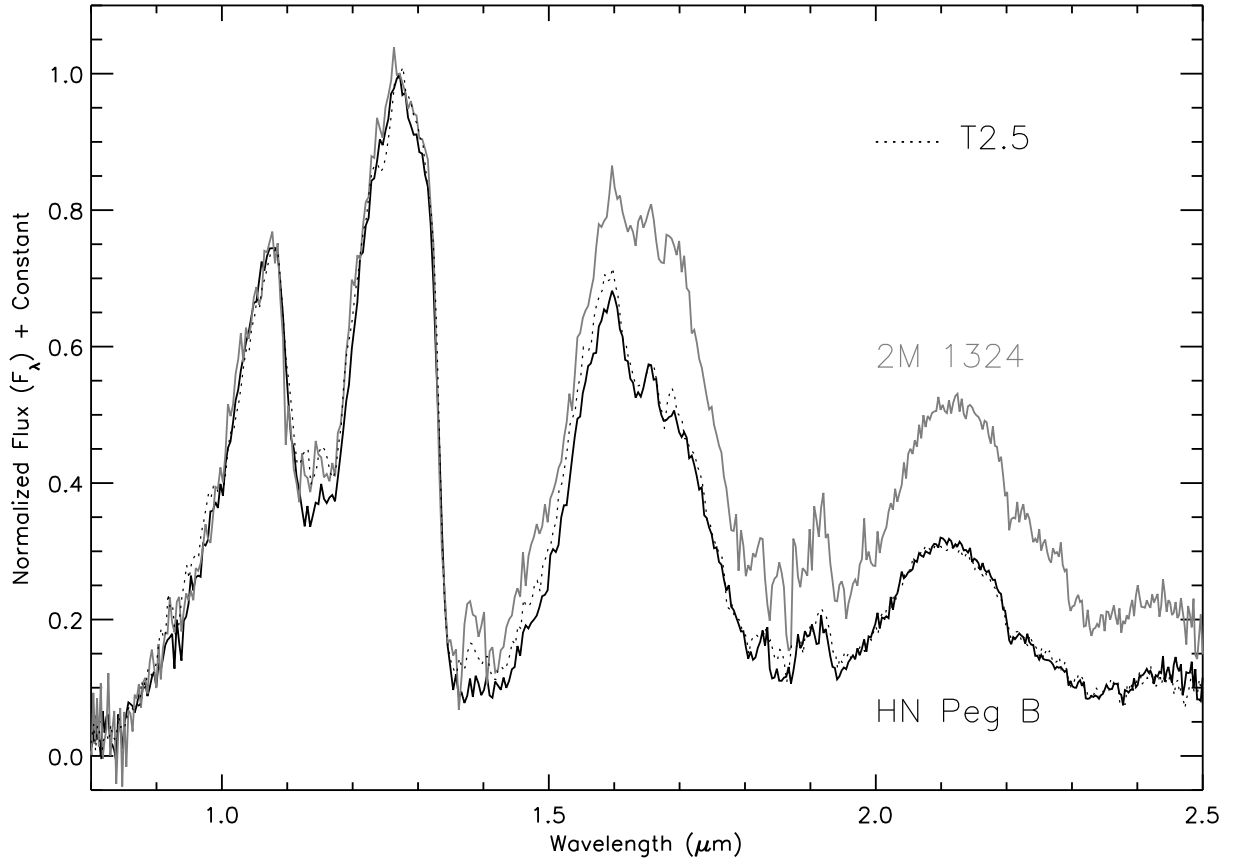
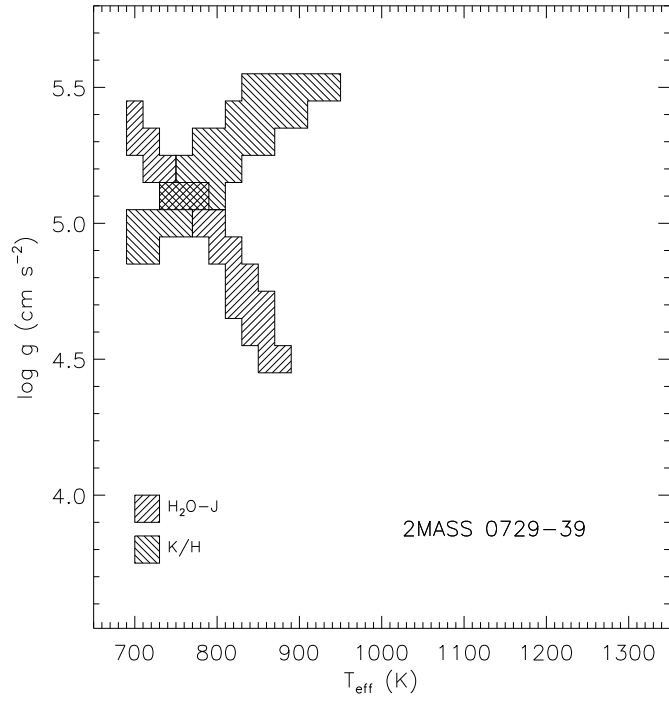
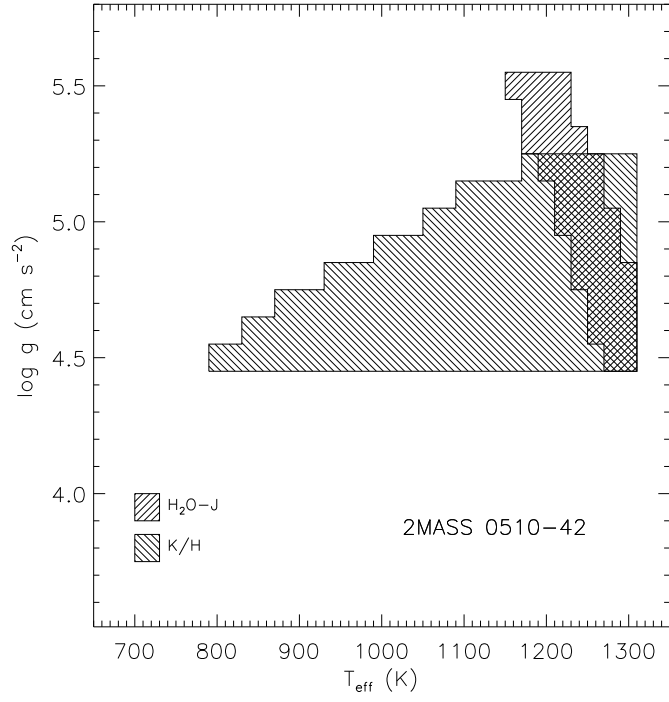
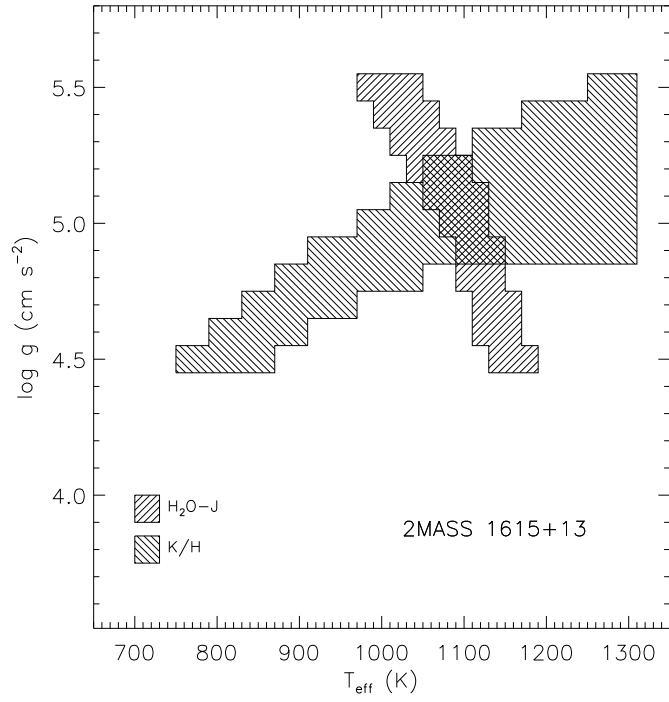
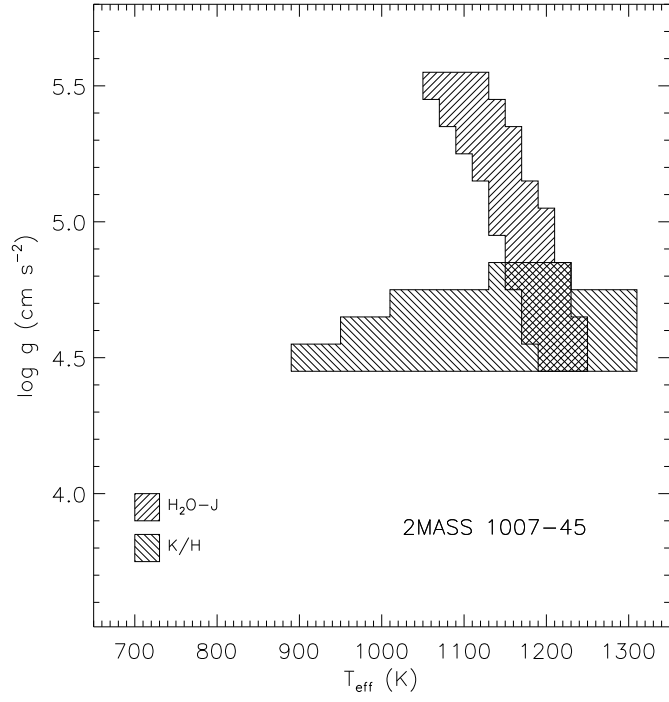


Fig. 8.— 2MASS 1324+63 (T2.5:pec, solid gray line) overplotted in comparison to HN Peg B (T2.5, solid black line, Luhman et al. 2007), an ~ 300 Myr old T dwarf. For comparison, a spectrum of a T2.5 dwarf constructed from the T2 and T3 spectral standards is also overplotted (dotted line). All spectra have been normalized at $1.27 \mu\text{m}$.





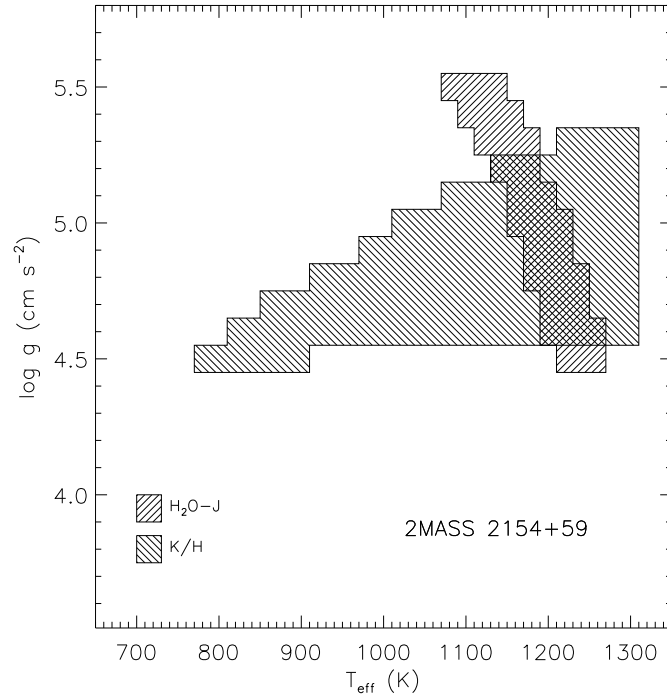


Fig. 9.— Spectral ratio measurements of H₂O and K/H (hatched regions) for 2MASS 0510–42 (T5), 2MASS 0729–39 (T8pec), 2MASS 1007–45 (T5), 2MASS 1615+13 (T6), and 2MASS 2154+59 (T5) shown in T_{eff} vs $\log g$ phase space. Overlapping regions are the best fits; we list these values in Table 8.

Table 1. Description of 2MASS Photometric Selection of T Dwarfs

Galactic Cut	J Mag Cut	Color Cuts	# of Candidates		Followed-up	Transients	M Dwarfs	T Dwarfs
			Cut 1 ^a	Cut 2 ^b				
$ b \geq 15^\circ$	$16 < J \leq 16.5^c$	$(J-H \leq 0)$ or $(J-H \leq 0.3, H-K_s \leq 0)$	13233	$67[+3]^d$	56	44	8	$4[+3]$
$10^\circ \leq b < 15^\circ$	$J \leq 16.5$	$(J-H \leq 0)$ or $(J-H \leq 0.3, H-K_s \leq 0)$	2719	8	6	4	1	1
$ b \leq 10^\circ, l \geq 20^\circ$	$J \leq 16$	$J-H \leq 0$	3711	6	5	2	0	3

^aInitial number of candidates from 2MASS Point Source Catalog.

^bCandidates remaining after visual inspection of DSS I & II images.

^c $J = 16.5$ has an SNR ~ 10 in the 2MASS Point Source Catalog, see Figure 7 in http://www.ipac.caltech.edu/2mass/releases/allsky/doc/sec2_2.html#pscphotprop.

^dThree previously known T dwarfs were identified.

Table 2. Transients

Object ^a	J ^b	H ^b	K _s ^b	UT Date ^c	β (deg) ^d
2MASS J00082060–1922267	16.26±0.09	15.99±0.17	16.04(null)	1998 Aug 14	–18.5
2MASS J00511030–0704476	16.30±0.09	16.03±0.13	16.19±0.36	1998 Oct 02	–11.6
2MASS J01085000–0428510	16.11±0.08	16.23±0.19	15.92±0.27	1998 Sep 18	–10.9
2MASS J01153773+2445277	16.46±0.12	16.16±0.22	16.16(null)	1997 Oct 31	+15.5
2MASS J01202541–0421252	16.41±0.12	16.25±0.25	17.03(null)	1998 Sep 20	–11.9
2MASS J01354860+1309260	16.41±0.11	16.44±0.23	16.21(null)	2000 Sep 24	+3.0
2MASS J02113209+1959189	16.19±0.09	15.90±0.13	15.99(null)	1997 Oct 19	+6.4
2MASS J02200443+1829383	16.36±0.12	16.07±0.17	16.33±0.39	1997 Oct 20	+4.3
2MASS J02215590+1943340	16.21±0.10	16.26±0.22	15.64±0.22	1997 Oct 20	+5.3
2MASS J02242110+1926020	16.37±0.11	16.62±0.29	15.57(null)	1997 Oct 20	+4.8
2MASS J02262810+2327310	16.21±0.10	16.29±0.21	15.49(null)	1997 Oct 20	+8.5
2MASS J02375362+2452399	16.19±0.09	15.93±0.15	16.01±0.25	1997 Nov 10	+9.0
2MASS J03532140–4154490	16.46±0.14	16.85±0.36	16.25(null)	1999 Sep 17	–59.9
2MASS J05314416–4224571	16.49±0.16	16.85±0.36	16.94(null)	1999 Oct 29	–65.5
2MASS J06550663+3024105	15.89±0.08	15.83±0.17	15.97±0.31	1998 Nov 23	+7.5
2MASS J08484742+0349184	16.36±0.15	16.40±0.28	16.91(null)	2000 Jan 29	–13.5
2MASS J09164433+0601113	16.31±0.13	16.24±0.24	16.83(null)	2000 Feb 22	–9.3
2MASS J10363196–1612231	16.27±0.11	16.03±0.15	16.34(null)	1998 Apr 02	–23.1
2MASS J11153870–0446599	16.42±0.10	16.92±0.30	16.95(null)	1999 Jan 04	–8.8
2MASS J11530357–2857301	16.42±0.15	16.74±0.36	16.75(null)	2000 Feb 01	–27.0
2MASS J12111689+1303508	16.31±0.11	16.05±0.18	16.52(null)	2000 Apr 05	+13.1
2MASS J12284242–1602593	16.44±0.12	16.28±0.19	16.80(null)	1998 Apr 01	–11.9
2MASS J12352384+2035252	16.14±0.10	15.89±0.18	15.89±0.24	1999 Apr 25	+22.3
2MASS J13175880–1427000	16.11±0.11	16.15±0.21	15.34(null)	1998 Apr 06	–5.8
2MASS J13271445–0819167	16.45±0.13	16.51±0.31	16.80(null)	1999 Feb 20	+0.8
2MASS J13343280–1952017	16.33±0.12	16.08±0.17	16.20(null)	1998 Apr 15	–9.3
2MASS J13502223–2210571	16.24±0.11	16.03±0.23	16.37(null)	1998 May 17	–10.1
2MASS J13540550+3139540	16.16±0.12	16.19±0.28	16.17(null)	1998 Mar 11	+40.0
2MASS J15452661–1418430	16.47±0.12	16.29±0.20	16.93(null)	1999 Mar 21	+5.4
2MASS J15470838–4111294	15.46±0.07	15.17±0.08	15.18±0.16	1999 May 14	–20.7
2MASS J16134510–3248360	15.56±0.07	15.63±0.14	15.36±0.21	1998 Jul 13	–11.4
2MASS J16490316+5357386	16.20±0.09	15.91±0.16	16.61(null)	1998 Jun 14	+74.8
2MASS J19404159+4752087	15.93±0.08	15.92±0.14	16.76(null)	1998 Jun 26	+67.2
2MASS J20043107–3710207	16.45±0.18	16.72±0.48	17.24(null)	1999 Jul 04	–16.4
2MASS J20320090–0749010	16.15±0.08	16.22±0.16	16.21(null)	1999 Jul 06	+10.7
2MASS J20574228–0515055	16.20±0.10	15.92±0.21	16.12(null)	1998 Sep 20	+11.5
2MASS J21000824+4759033	15.79±0.08	15.93±0.15	14.72(null)	2000 Jun 10	+60.4
2MASS J21150144–4526057	16.34±0.11	16.36±0.26	17.23(null)	1999 Aug 13	–28.0
2MASS J21290545+4159005	15.60±0.06	16.09±0.20	15.29±0.16	2000 May 18	+52.6
2MASS J21542683+2116188	16.37±0.12	16.22±0.24	16.41(null)	1999 Oct 02	+31.7
2MASS J21573780–2047520	16.49±0.12	16.55±0.24	16.04(null)	1998 Aug 11	–7.8
2MASS J22003181–2301592	16.43±0.14	16.34±0.28	16.96(null)	1998 Jul 04	–10.2
2MASS J22152050+1316290	16.46±0.13	16.25±0.19	16.47(null)	1997 Sep 13	+22.4
2MASS J22155422–2526573	16.14±0.11	15.85±0.14	16.08(null)	2000 Jul 24	–13.7
2MASS J22423443–0420011	16.39±0.10	16.18±0.18	16.46(null)	1998 Sep 29	+3.6
2MASS J22523538+2359146	16.20±0.11	15.91±0.20	15.94(null)	1997 Oct 06	+28.6

Table 2—Continued

Object ^a	J ^b	H ^b	K _s ^b	UT Date ^c	β (deg) ^d
2MASS J23170461–0622477	16.13±0.09	15.96±0.19	16.15(null)	1998 Oct 10	–1.6
2MASS J23314348+1519291	16.39±0.12	16.22±0.20	16.32(null)	1997 Sep 29	+16.8
2MASS J23315967+1602183	16.29±0.12	16.26±0.21	16.85(null)	1997 Sep 29	+17.5
2MASS J23335590–0441137	16.04±0.07	15.77±0.12	15.87±0.23	2000 Sep 17	–1.7

^aJ2000 coordinates from the 2MASS All-Sky Point Source Catalog.

^bPhotometry from 2MASS All-Sky Point Source Catalog.

^cUT date of 2MASS observation.

^d β : Ecliptic latitude.

Table 3. IRTF/SpEx-prism Log

Object ^a	J ^b	H ^b	K _s ^b	UT Date	AM ^c	N × t(s) ^d	SpT	b/β (deg) ^e	Calibrator
2MASS J01072340+4759060	15.90±0.08	16.11±0.18	15.68±0.19	2006 Aug 17	1.15	8×120	M3	−14.8°/+37.2°	HD 9711 (A0 V)
2MASS J05063725−3405090	16.36±0.13	16.06±0.19	16.22(null)	2006 Dec 08	1.70	8×120	M7	−35.5°/−56.6°	HD 29028 (A0 V)
2MASS J05103520−4208140	16.22±0.09	16.24±0.16	16.00±0.28	2006 Sep 02	2.37	4×120	T5	−35.9°/−64.6°	HD 38921 (A0 V)
2MASS J05273570−1813490	16.49±0.23	16.53±0.39	15.16(null)	2006 Sep 01	1.56	8×120	M4	−26.4°/−41.4°	HD 37190 (A0 V)
2MASS J06020638+4043588	15.54±0.07	15.59±0.14	15.17±0.16	2006 Dec 09	1.07	8×120	T4.5	+8.8°/+17.3°	HD 39250 (A0 V)
2MASS J07290002−3954043	15.92±0.08	15.98±0.19	15.29(null)	2006 Dec 08	2.00	16×120	T8.0pec	−10.4°/−60.6°	HD 61516 (A0 V)
SDSSp J083717.22−000018.3	17.10±0.21	15.99±0.17	15.67(null)	2006 Dec 21	1.08	20×180	T1 std	+23.4°/−17.9°	HD 74721 (A0 V)
2MASS J09162680+0628390	16.25±0.14	16.29±0.26	15.71(null)	2006 Dec 09	1.03	4×120	M6.5	+35.1°/−8.9°	HD 79108 (A0 V)
2MASS J09212890−0339410	16.46±0.14	16.53±0.30	15.90(null)	2006 Dec 09	1.12	8×120	M7:	+30.8°/−18.2°	HD 79108 (A0 V)
2MASS J09351549+0019103	16.47±0.15	16.27±0.20	16.61(null)	2006 Dec 21	1.11	4×120	M7:	+35.9°/−13.3°	HD 74721 (A0 V)
2MASS J10073369−4555147	15.65±0.07	15.69±0.12	15.56±0.23	2006 Dec 09	2.45	8×120	T5	+8.0°/−52.1°	HD 88113 (A0 V)
2MASS J11061197+2754225	14.82±0.04	14.15±0.05	13.80±0.05	2006 Apr 08	1.03	8×120	T2.5	+66.7°/+20.3°	HD 89239 (A0 V)
SDSS J120747.17+024424.8	15.58±0.07	14.56±0.07	13.99±0.06	2006 Dec 20	1.21	8×120	T0 std	+63.5°/+3.3°	HD 111744 (A0 V)
2MASS J12154432−3420591	16.24±0.13	15.81±0.19	16.32(null)	2006 May 31	2.05	8×120	T4.5	+27.9°/−29.7°	SAO 203194 (A0 V)
2MASS J13243559+6358284	15.60±0.07	14.58±0.06	14.06±0.07	2006 Apr 11	1.49	6×150	T2.5	+52.8°/+62.6°	HD 118214 (A0 V)
2MASS J14044941−3159329	15.58±0.07	14.96±0.08	14.54±0.10	2006 Jun 01	2.18	12×120	T2.5	+28.4°/−18.1°	SAO 205525 (A0 V)
2MASS J16150413+1340079	16.35±0.09	16.49±0.25	15.86(null)	2006 Sep 02	1.10	16×120	T6	+48.8°/+34.3°	q Her (A0 V)
2MASS J16293700+1415440	16.27±0.11	16.36±0.26	15.00±0.15	2006 Sep 02	1.32	4×120	M6:	+37.8°/+35.6°	q Her (A0 V)
2MASS J20014670−3805400	16.42±0.11	16.44±0.23	15.87(null)	2006 Sep 01	2.10	8×120	M4	−29.5°/−17.2°	HD 189501 (A0 V)
2MASS J21542494−1023022	16.43±0.12	16.45±0.28	17.05(null)	2006 Aug 17	1.28	8×120	T4.5	−45.2°/+2.2°	HD 211278 (A0 V)
2MASS J21543318+5942187	15.66±0.07	15.77±0.17	15.34(null)	2006 Nov 17	1.41	12×180	T5	+4.1°/+63.7°	BD+62 2148 (A0 V)
2MASS J22535460−0321450	16.01±0.09	16.09±0.22	15.46±0.23	2006 Aug 18	1.16	8×120	M6	−53.2°/+3.4°	HD 216807 (A0 V)

^aJ2000 coordinates from the 2MASS All-Sky Point Source Catalog.

^bPhotometry from 2MASS All-Sky Point Source Catalog.

^cAM: Airmass.

^dNumber of integrations times integration time.

^eb: Galactic latitude, β: Ecliptic latitude.

Table 4. Spectrophotometric Properties of New and Confirmed T Dwarfs

Object	J ^a	J–H ^a	H–K _s ^a	J–K _s ^a	i ^b	z ^b	SpT	Distance (pc) ^c
New T Dwarfs								
2MASS J05103520–4208140	16.22±0.09	–0.02±0.18	0.24±0.32	0.23±0.30	T5	24.3±2.0
2MASS J06020638+4043588	15.54±0.07	–0.05±0.15	0.43±0.21	0.38±0.17	T4.5	19.3±1.5
2MASS J07290002–3954043	15.92±0.08	–0.06±0.20	< 0.69	< 0.63	T8 _{pec}	8.4±0.7
2MASS J10073369–4555147	15.65±0.07	–0.04±0.14	0.13±0.26	0.09±0.24	T5	18.7±1.4
2MASS J11061197+2754225	14.82±0.04	0.67±0.06	0.35±0.07	1.02±0.06	21.28±0.09	17.70±0.03	T2.5	15.5±1.2
2MASS J12154432–3420591	16.24±0.13	0.43±0.23	< –0.51	< –0.08	T4.5	26.6±2.1
2MASS J13243559+6358284	15.60±0.07	1.02±0.10	0.52±0.09	1.54±0.10	22.68±0.26	18.73±0.04	T2:pec	21.8±1.7
2MASS J14044941–3159329	15.58±0.07	0.62±0.10	0.42±0.12	1.04±0.12	T2.5	22.0±1.7
2MASS J16150413+1340079	16.35±0.09	–0.14±0.27	< 0.63	< 0.49	...	19.90±0.09	T6	20.4±1.6
2MASS J21542494–1023022	16.43±0.12	–0.03±0.30	< –0.59	< –0.62	T4.5	29.0±2.3
2MASS J21543318+5942187	15.66±0.07	–0.10±0.18	< 0.43	< 0.32	T6	18.8±1.5
Recovered T Dwarfs								
2MASS J09393548–2448279 ^d	15.98±0.11	0.18±0.18	< –0.76	< –0.58	T8 ^e	8.7±0.7
SDSSp J134646.45–003150.4 ^d	16.00±0.10	0.54±0.16	–0.31±0.30	0.23±0.29	T6.5 ^e	15.0±1.2
SDSS J163022.92+081822.0 ^d	16.40±0.11	0.07±0.31	< –0.28	< –0.21	23.82±0.61	20.13±0.10	T5.5 ^e	23.7±1.8
SDSS J175805.46+463311.9 ^d	16.15±0.09	–0.10±0.24	0.79±0.29	0.69±0.21	24.18±0.57	19.67±0.07	T6.5 ^e	16.1±1.2
SDSS J212413.89+010000.3 ^d	16.03±0.07	–0.15±0.21	< 0.04	< –0.11	23.77±0.54	19.71±0.12	T5 ^e	22.3±1.7

^aPhotometry from 2MASS All-Sky Point Source Catalog.

^bPhotometry from SDSS (AB) Data Release 5.

^cSpectrophotometric distance estimates derived in §3.2.1.

^dReferences: 2MASS 0939–24 (Tinney et al. 2005), SDSS 1346–00 (Tsvetanov et al. 2000), SDSS 1630+08 (Chiu et al. 2006), SDSS 1758+46 (Knapp et al. 2004), SDSS 2124+01 (Knapp et al. 2004).

^eBurgasser et al. (2006a).

Table 5. Spectral Indices of 11 New T Dwarfs^a

Object	H ₂ O- <i>J</i>	CH ₄ - <i>J</i>	H ₂ O- <i>H</i>	CH ₄ - <i>H</i>	CH ₄ - <i>K</i>	H ₂ O- <i>K</i>	<i>K/J</i>	Derived NIR SpT	
								Direct ^{b,c}	Ind 1 ^{c,d,e}
2MASS J1324+63	0.431 (T2.5)	0.529 (T3)	0.485 (T2)	1.006 (L9.5)	0.665 (T1.5)	0.589	0.501	T2:pec	T1.5:
2MASS J1106+27	0.481 (T2)	0.564 (T2.5)	0.522 (T1.5)	0.781 (T2.5)	0.614 (T2)	0.585	0.336	T2.5	T2
2MASS J1404–31	0.442 (T2.5)	0.522 (T3)	0.506 (T1.5)	0.749 (T3)	0.649 (T1.5)	0.613	0.312	T2.5	T2.5
2MASS J2154–10	0.349 (T4)	0.438 (T4.5)	0.395 (T4)	0.524 (T4.5)	0.273 (T4.5)	0.498	0.212	T4.5	T4.5
2MASS J0602+40	0.303 (T4.5)	0.433 (T4.5)	0.363 (T4.5)	0.457 (T4.5)	0.240 (T4.5)	0.469	0.181	T4.5	T4.5
2MASS J1215–34	0.308 (T4.5)	0.486 (T4)	0.382 (T4)	0.414 (T5)	0.151 (T6)	0.536	0.225	T4.5	T4.5
2MASS J0510–42	0.261 (T5)	0.414 (T4.5)	0.337 (T5)	0.348 (T5.5)	0.125 (T6.5)	0.459	0.189	T5	T5.5
2MASS J2154+59	0.217 (T5.5)	0.354 (T6)	0.325 (T5.5)	0.361 (T5.5)	0.163 (T5.5)	0.437	0.167	T5	T5.5
2MASS J1007–45	0.205 (T5.5)	0.360 (T5)	0.310 (T5.5)	0.314 (T6)	0.151 (T6)	0.402	0.199	T5	T5.5
2MASS J1615+13	0.167 (T6)	0.313 (T6.5)	0.305 (T5.5)	0.267 (T6.5)	0.153 (T6)	0.399	0.145	T6	T6
2MASS J0729–39	0.053 (T7.5)	0.251 (T7)	0.175 (>T8)	0.202 (T7)	0.044 (>T8)	0.325	0.091	T8pec	T7

^aNIR indices are defined by Burgasser et al. (2006a).

^bDirect spectral typing is done by visually comparing objects against standards.

^cColons mark estimates with standard deviations ≥ 1 spectral type.

^dIndex values outside the proscribed range (i.e., '<' or '>') are not used to compute the average spectral type.

^eSpectral typing follows the convention of Burgasser et al. (2006a), where Ind 1 (in parentheses) is computed by comparison of the indices to the indices of standards.

Table 6. Kinematic Properties of 4 T Dwarfs with Multi-Epoch Measurements

Object	SpT	μ (″/yr)	θ (deg)	Δt (yr)	Dist (pc)	V_{tan}^a (km s ⁻¹)
2MASS 1106+27 ^b	T2.5	0.57±0.08	216.6±0.3	2.13	15.5±1.2	42±2
2MASS 1324+63 ^b	T2:pec	0.43±0.08	232.8±0.3	1.04	21.8±1.7	45±3
2MASS 1404–31 ^b	T2.5	0.35±0.03	275.3±0.2	2.55	22.0±1.7	36±2
2MASS 1615+13 ^c	T6	0.48±0.05	139.0±0.2	6.22	29.0±2.3	66±4

^a $V_{tan} = 4.74 \times D \times \mu'$ and $\sigma_{V_{tan}} = \sqrt{(4.74 (\mu' \times \sigma_D^2 + D \times \sigma_{\mu'}^2))}$, where $\mu' = \mu \times 1 \text{ yr [″]}$.

^bBoth epochs are from the 2MASS Working Database.

^cThe first epoch is from the 2MASS Point Source Catalog, and the second epoch is from the SDSS Catalog.

Table 7. Synthetic Spectral Indices^a

SpT of A+B	Derived NIR SpT								
	H ₂ O- <i>J</i>	CH ₄ - <i>J</i>	H ₂ O- <i>H</i>	CH ₄ - <i>H</i>	CH ₄ - <i>K</i>	H ₂ O- <i>K</i>	<i>K</i> / <i>J</i>	Direct ^{b,c}	Ind 1 ^{b,d,e}
L8 std	0.706 (L8)	0.735 (L8)	0.705 (L8)	1.077 (L8)	0.881 (L8)	0.696	0.743	L8	L8
L8+L9	0.666 (L8.5)	0.705 (L8.5)	0.661 (L8.5)	1.085 (<L8)	0.887 (<L8)	0.697	0.688	L8.5	L8.5
L8+T0	0.657 (L8.5)	0.685 (L9)	0.655 (L8.5)	1.012 (L9.5)	0.840 (L9.5)	0.689	0.570	L9	L9
L8+T1	0.630 (L9)	0.683 (L9)	0.625 (L9)	1.023 (L9.5)	0.807 (T0)	0.660	0.525	L9.5	L9.5
L8+T2	0.550 (T1.5)	0.631 (T1.5)	0.566 (T1)	0.981 (T1)	0.732 (T1)	0.624	0.490	T0	T1
L8+T3	0.502 (T1.5)	0.582 (T2)	0.554 (T1)	0.862 (T2.5)	0.712 (T1)	0.618	0.413	T1	T1.5
L8+T4	0.478 (T2)	0.580 (T2)	0.527 (T1.5)	0.798 (T2.5)	0.652 (T1.5)	0.611	0.404	T1.5:	T2
L8+T5	0.407 (T3)	0.492 (T4)	0.542 (T1)	0.767 (T2.5)	0.705 (T1)	0.631	0.367	T2:	T2.5:
L8+T6	0.404 (T3)	0.526 (T3)	0.554 (T1)	0.802 (T2.5)	0.750 (T0.5)	0.644	0.418	T2:	T2:
L8+T7	0.447 (T2.5)	0.528 (T3)	0.585 (T0.5)	0.853 (T2.5)	0.775 (T0)	0.648	0.504	T1:	T1.5:
L8+T8	0.522 (T1.5)	0.583 (T2)	0.620 (L9)	0.919 (T2)	0.833 (L9.5)	0.672	0.577	T0:	T1:
L9 std	0.631 (L9)	0.681 (L9)	0.621 (L9)	1.092 (L9)	0.894 (L9)	0.698	0.640	L9	L9
L9+T0	0.626 (L9.5)	0.664 (L9.5)	0.616 (L9.5)	1.022 (L9.5)	0.847 (L9.5)	0.690	0.533	L9.5	L9.5
L9+T1	0.604 (T0.5)	0.664 (L9.5)	0.589 (T0.5)	1.032 (L9.5)	0.815 (T0)	0.661	0.494	L9.5	T0
L9+T2	0.531 (T1.5)	0.618 (T1.5)	0.535 (T1.5)	0.990 (L9.5)	0.740 (T1)	0.625	0.464	T0.5	T1
L9+T3	0.486 (T2)	0.571 (T2)	0.523 (T1.5)	0.875 (T2)	0.721 (T1)	0.619	0.392	T1.5	T1.5
L9+T4	0.463 (T2)	0.567 (T2)	0.495 (T2)	0.815 (T2.5)	0.662 (T1.5)	0.613	0.383	T2	T2
L9+T5	0.394 (T3.5)	0.484 (T4)	0.502 (T1.5)	0.789 (T2.5)	0.717 (T1)	0.633	0.345	T2.5:	T2.5:
L9+T6	0.387 (T3.5)	0.514 (T3)	0.506 (T1.5)	0.826 (T2.5)	0.762 (T0.5)	0.646	0.387	T2.5:	T2:
L9+T7	0.422 (T3)	0.511 (T3.5)	0.528 (T1.5)	0.878 (T2)	0.788 (T0)	0.650	0.459	T2:	T2:
L9+T8	0.485 (T2)	0.558 (T2.5)	0.555 (T1)	0.942 (T1.5)	0.846 (L9.5)	0.675	0.515	T1:	T1.5:
T0 std	0.621 (T0)	0.651 (T0)	0.612 (T0)	0.955 (T0)	0.790 (T0)	0.680	0.442	T0	T0
T0+T1	0.602 (T0.5)	0.651 (T0)	0.585 (T0.5)	0.969 (T0)	0.755 (T0.5)	0.648	0.414	T0.5	T0.5
T0+T2	0.533 (T1.5)	0.610 (T1.5)	0.533 (T1.5)	0.933 (T1.5)	0.677 (T1.5)	0.610	0.396	T1	T1.5
T0+T3	0.491 (T2)	0.566 (T2.5)	0.521 (T1.5)	0.820 (T2.5)	0.647 (T1.5)	0.601	0.332	T2	T2
T0+T4	0.469 (T2)	0.562 (T2.5)	0.493 (T2)	0.756 (T3)	0.574 (T2)	0.592	0.320	T2.5:	T2.5
T0+T5	0.405 (T3)	0.483 (T4)	0.499 (T1.5)	0.718 (T3)	0.615 (T2)	0.610	0.279	T3	T2.5
T0+T6	0.402 (T3)	0.511 (T3.5)	0.504 (T1.5)	0.742 (T3)	0.656 (T1.5)	0.623	0.303	T3:	T2.5
T0+T7	0.436 (T2.5)	0.508 (T4)	0.524 (T1.5)	0.779 (T2.5)	0.679 (T1.5)	0.626	0.347	T2:	T2.5:
T0+T8	0.495 (T2)	0.548 (T2.5)	0.549 (T1)	0.831 (T2.5)	0.739 (T1)	0.653	0.376	T1:	T2
T1 std	0.584 (T1)	0.653 (T1)	0.563 (T1)	0.981 (T1)	0.724 (T1)	0.620	0.391	T1	T1
T1+T2	0.523 (T1.5)	0.613 (T1.5)	0.515 (T1.5)	0.947 (T1.5)	0.650 (T1.5)	0.584	0.377	T1.5	T1.5
T1+T3	0.485 (T2)	0.573 (T2)	0.504 (T1.5)	0.840 (T2.5)	0.616 (T2)	0.572	0.318	T2	T2
T1+T4	0.464 (T2)	0.570 (T2)	0.476 (T2)	0.782 (T2.5)	0.545 (T2.5)	0.561	0.307	T2.5	T2
T1+T5	0.406 (T3)	0.499 (T4)	0.478 (T2)	0.752 (T3)	0.576 (T2)	0.571	0.267	T3	T3
T1+T6	0.402 (T3)	0.526 (T3)	0.478 (T2)	0.778 (T2.5)	0.610 (T2)	0.578	0.287	T3	T2.5
T1+T7	0.433 (T2.5)	0.528 (T3)	0.494 (T2)	0.817 (T2.5)	0.629 (T1.5)	0.578	0.323	T2.5	T2.5
T1+T8	0.483 (T2)	0.565 (T2.5)	0.513 (T1.5)	0.867 (T2.5)	0.680 (T1.5)	0.599	0.343	T2	T2
T2 std	0.474 (T2)	0.583 (T2)	0.474 (T2)	0.917 (T2)	0.585 (T2)	0.552	0.365	T2	T2
T2+T3	0.442 (T2.5)	0.547 (T2.5)	0.463 (T2.5)	0.818 (T2.5)	0.546 (T2.5)	0.537	0.312	T2.5	T2.5
T2+T4	0.422 (T3)	0.544 (T2.5)	0.435 (T3.5)	0.763 (T3)	0.474 (T3)	0.524	0.302	T3	T3
T2+T5	0.365 (T4)	0.477 (T4)	0.429 (T3.5)	0.732 (T3)	0.486 (T3)	0.525	0.266	T3	T3.5
T2+T6	0.356 (T4)	0.498 (T4)	0.423 (T3.5)	0.754 (T3)	0.507 (T3)	0.527	0.283	T3	T3.5

Table 7—Continued

SpT of A+B								Derived NIR SpT	
	H ₂ O- <i>J</i>	CH ₄ - <i>J</i>	H ₂ O- <i>H</i>	CH ₄ - <i>H</i>	CH ₄ - <i>K</i>	H ₂ O- <i>K</i>	<i>K/J</i>	Direct ^{b,c}	Ind 1 ^{b,d,e}
T2+T7	0.373 (T4)	0.494 (T4)	0.429 (T3.5)	0.785 (T2.5)	0.518 (T3)	0.524	0.313	T3	T3.5
T2+T8	0.407 (T3)	0.521 (T3)	0.441 (T3)	0.825 (T2.5)	0.554 (T2.5)	0.537	0.329	T2.5	T3
T3 std	0.413 (T3)	0.516 (T3)	0.453 (T3)	0.717 (T3)	0.496 (T3)	0.519	0.264	T3	T3
T3+T4	0.392 (T3.5)	0.510 (T3.5)	0.423 (T3.5)	0.654 (T3.5)	0.408 (T3.5)	0.503	0.252	T3.5	T3.5
T3+T5	0.337 (T4)	0.445 (T4.5)	0.414 (T3.5)	0.602 (T4)	0.405 (T3.5)	0.497	0.215	T4	T4
T3+T6	0.323 (T4.5)	0.459 (T4.5)	0.406 (T3.5)	0.606 (T4)	0.420 (T3.5)	0.497	0.222	T4	T4
T3+T7	0.334 (T4.5)	0.449 (T4.5)	0.411 (T3.5)	0.619 (T3.5)	0.427 (T3.5)	0.490	0.240	T4	T4
T3+T8	0.359 (T4)	0.468 (T4.5)	0.422 (T3.5)	0.647 (T3.5)	0.464 (T3)	0.503	0.245	T3.5	T3.5
T4 std	0.369 (T4)	0.506 (T4)	0.389 (T4)	0.581 (T4)	0.305 (T4)	0.482	0.239	T4	T4
T4+T5	0.310 (T4.5)	0.437 (T4.5)	0.372 (T4.5)	0.508 (T4.5)	0.269 (T4.5)	0.471	0.199	T4.5	T4.5
T4+T6	0.291 (T4.5)	0.450 (T4.5)	0.356 (T4.5)	0.498 (T4.5)	0.266 (T4.5)	0.466	0.204	T4.5	T4.5
T4+T7	0.297 (T4.5)	0.438 (T4.5)	0.355 (T5)	0.499 (T4.5)	0.260 (T4.5)	0.455	0.220	T4.5	T4.5
T4+T8	0.319 (T4.5)	0.456 (T4.5)	0.362 (T4.5)	0.518 (T4.5)	0.283 (T4)	0.467	0.223	T4	T4.5
T5 std	0.240 (T5)	0.356 (T5)	0.345 (T5)	0.393 (T5)	0.200 (T5)	0.450	0.151	T5	T5
T5+T6	0.205 (T5.5)	0.355 (T5.5)	0.319 (T5.5)	0.357 (T5.5)	0.180 (T5.5)	0.438	0.148	T5.5	T5.5
T5+T7	0.195 (T5.5)	0.322 (T6.5)	0.311 (T5.5)	0.332 (T5.5)	0.159 (T6)	0.417	0.155	T5.5	T6
T5+T8	0.205 (T5.5)	0.325 (T6.5)	0.315 (T5.5)	0.338 (T5.5)	0.177 (T5.5)	0.428	0.148	T5.5	T5.5
T6 std	0.154 (T6)	0.354 (T6)	0.280 (T6)	0.301 (T6)	0.149 (T6)	0.418	0.142	T6	T6
T6+T7	0.129 (T6.5)	0.311 (T6.5)	0.259 (T6.5)	0.256 (T6.5)	0.114 (T6.5)	0.387	0.150	T6.5	T6.5
T6+T8	0.127 (T6.5)	0.313 (T6.5)	0.255 (T6.5)	0.250 (T6.5)	0.127 (T6.5)	0.394	0.140	T6.5	T6.5
T7 std	0.085 (T7)	0.238 (T7)	0.224 (T7)	0.181 (T7)	0.062 (T7)	0.340	0.164	T7	T7
T7+T8	0.070 (T7.5)	0.219 (T7.5)	0.209 (T7.5)	0.153 (T7.5)	0.059 (T7)	0.332	0.152	T7.5	T7.5
T8 std	0.041 (T8)	0.182 (T8)	0.183 (T8)	0.104 (T8)	0.050 (T8)	0.311	0.131	T8	T8

^aNIR indices are defined by Burgasser et al. (2006a).

^bColons mark estimates with standard deviations ≥ 1 spectral type.

^cDirect spectral typing is done by visually comparing objects against standards.

^dIndex values outside the proscribed range (i.e., '<' or '>') are not used to compute the average spectral type.

^eSpectral typing follows the convention of Burgasser et al. (2006a), where Ind 1 (in parentheses) is computed by comparison of the indices to the indices of standards.

Table 8. T_{eff} and Log g Estimates for Late-Type T Dwarfs

Object	SpT	T_{eff} [K]	log g [cgs]	Mass [M_{\odot}]	Age [Gyr]
2MASS 0510–42	T5	1200–1300	4.5–5.2	0.017–0.049	0.13–2.1
2MASS 0729–39	T8pec	740–780	5.1	0.038–0.039	3.8–4.1
2MASS 1007–45	T5	1160–1240	4.5–4.8	0.017–0.027	0.2–0.4
2MASS 1615+13	T6	1060–1140	4.9–5.2	0.030–0.048	0.6–2.9
2MASS 2154+59	T5	1140–1240	4.7–5.2	0.023–0.048	0.3–2.5

Table 9. T Dwarfs in the Solar Neighborhood (within 25 pc)

Name of T Dwarf	Discovery Reference ^c	NIR SpT	J^a (mag)	K_s^a (mag)	Distance (pc)			High-res imaging?	Follow-up Reference ^c	Remarks
					from J	from π_{trig}	Adopted Distance ^b			
ϵ Indi Bab (2MASS J2204–5646)	1	T1.0/T6.0	12.29	11.35	4.45	3.63	3.6	Yes	28	binary: a=0''732
SCR J1845–6357B	2	T5.5	13.16 ^d	3.85	3.9	Yes	2	single
2MASSI J0415195–093506	3	T8.0	15.70	15.43	7.58	5.74	5.7	Yes	29	single
Gl 229B (J0610–2152)	4	T7.0p	14.20	14.30	5.53	5.77	5.8	Yes	4,30	single
Gl 570D (2MASS J1457–2121)	5	T7.5	15.32	15.24	7.73	5.91	5.9	Yes	31	single
2MASSI J0937347+293142	3	T6.0p	14.65	15.27	9.32	6.14	6.1	Yes	31	single
IPMS J013656.57+093347.3	6	T2.5	13.46	12.56	8.27	...	8.3	No	...	single
2MASS J07290002–3954043	7	T8.0p	15.92	...	8.41	...	8.4	No
2MASS J15031961+2525196	8	T5.0	13.94	13.96	8.49	...	8.5	Yes	29	single
2MASS J09393548–2448279	9	T8.0	15.98	...	8.65	...	8.7	No
2MASSI J0727182+171001	3	T7.0	15.60	15.56	10.53	9.08	9.1	No
2MASS J03480772–6022270	10	T7.0	15.32	15.60	9.25	...	9.3	Yes	29	single
2MASS J11145133–2618235	9	T7.5	15.86	...	9.89	...	9.9	No
2MASS J05591914–1404488	11	T4.5	13.80	13.58	8.66	10.24	10.2	Yes	31	single
2MASS J12373919+6526148	12	T6.5	16.05	...	15.33	10.41	10.4	Yes	31	single
2MASSI J1047538+212423	12	T6.5	15.82	...	13.76	10.56	10.6	Yes	31	single
2MASSI J0243137–245329	3	T6.0	15.38	15.22	13.06	10.68	10.7	Yes	29	single
SDSSp J162414.37+002915.6	13	T6.0	15.49	...	13.76	11.00	11.0	Yes	29	single
2MASSI J1217110–031113	12	T7.5	15.86	...	9.90	11.01	11.0	Yes	29,27	single
HD 3651B (J0039+2115)	14	T8	16.16 ^d	16.87 ^d	9.39	11.11	11.1	No
2MASSI J1546291–332511	3	T5.5	15.63	15.49	16.66	11.36	11.4	Yes	31	single
2MASSI J1553022+153236AB	3	T7.0	15.83	15.51	11.68	...	>11.7	Yes	29	binary: a=0''349
SDSSp J125453.90–012247.4	15	T2.0	14.89	13.84	15.76	11.78	11.8	Yes	29	single
2MASS J00345157+0523050	16	T6.5	15.54	...	12.08	...	12.1	No
2MASS J00501994–3322402	9	T7.0	15.93	15.24	12.24	...	12.2	No
2MASS J12255432–2739466AB	12	T6.0	15.26	15.07	12.35	13.32	13.3	Yes	31	binary: a=0''282
2MASS J18283572–4849046	16	T5.5	15.18	15.18	13.50	...	13.5	No
2MASSI J1534498–295227AB	3	T5.5	14.90	14.84	11.90	13.59	13.6	Yes	31	binary: a=0''65
2MASSI J2356547–155310	3	T5.5	15.82	15.77	18.21	14.50	14.5	Yes	31	single
SDSSp J134646.45–003150.4	17	T6.5	16.00	15.77	14.96	14.64	14.6	No
2MASS J22282889–4310262	10	T6.0	15.66	15.30	14.86	...	14.9	Yes	29	single
SDSSp J042348.57–041403.5AB	18	T0.0	14.47	12.93	11.10	15.17	15.2	Yes	29	binary: a=0''164

Table 9—Continued

Name of T Dwarf	Discovery Reference ^c	NIR SpT	J^a (mag)	K_s^a (mag)	Distance (pc)		Adopted Distance ^b	High-res imaging?	Follow-up Reference ^c	Remarks
					from J	from π_{trig}				
SDSS J000013.54+255418.6	19	T4.5	15.06	14.84	15.48	...	15.5	No
2MASS J11061197+2754225	7	T2.5	14.82	13.80	15.51	...	15.5	No
SDSS J162838.77+230821.1	20	T7.0	16.46	15.87	15.63	...	15.6	No
SDSS J175805.46+463311.9	19	T6.5	16.15	15.47	16.05	...	16.1	No
SDSS J075840.33+324723.4	19	T2.0	14.95	13.88	16.17	...	16.2	No
2MASS J12314753+0847331	16	T5.5	15.57	15.22	16.20	...	16.2	No
2MASS J11220826-3512363	9	T2.0	15.02	14.38	16.72	...	16.7	No
2MASS J2254188+312349	3	T4.0	15.26	14.90	18.01	...	18.0	Yes	29	single
2MASS J21392676+0220226	21	T1.5	15.26	13.58	18.18	...	18.2	No
SDSS J152039.82+354619.8	20	T0.0	15.54	14.00	18.21	...	18.2	No
HN Peg B (J2144+1446)	22	T2.5	15.86 ^e	15.12 ^e	25.03	18.39	18.4			
SDSS J120747.17+024424.8	23	T0.0	15.58	13.99	18.54	...	18.5	No
2MASS J10073369-4555147	7	T5.0	15.65	15.56	18.68	...	18.7	No
2MASS J23312378-4718274	16	T5.0	15.66	15.39	18.76	...	18.8	No
2MASS J21543318+5942187	7	T5.0	15.66	...	18.78	...	18.8	No
2MASSW J0920122+351742AB	24	T0.0	15.63	13.98	18.93	...	>18.9	Yes	32	binary: a=0''07
2MASS J06020638+4043588	7	T4.5	15.54	15.12	19.32	...	19.3	No
2MASS J0755480+221218	3	T5.0	15.728	15.75	19.36	...	19.4	Yes	29	single
2MASS J05160945-0445499	10	T5.5	15.98	15.49	19.60	...	19.6	Yes	29	single
SDSS J150411.63+102718.4	20	T7.0	17.03	17.02	20.36	...	20.4	No
2MASS J16150410+1340070	7	T6.0	16.35	...	20.40	...	20.4	No
GI 337CD (2MASS J0912+1459)	25	T0.0	15.51	14.04	17.97	20.48	20.5	Yes	33	binary: a=0''53
2MASS J19010601+4718136	16	T5.0	15.86	15.64	20.54	...	20.5	No
SDSS J015141.69+124429.6	18	T1.0	16.57	15.18	31.89	21.40	21.4	Yes	29	single
2MASS J13243559+6358284	7	T2.0p	15.60	14.06	21.80	...	21.8	No
2MASS J14044941-3159329	7	T2.5	15.58	14.54	21.97	...	22.0	No
SDSS J032553.17+042540.1	20	T5.5	16.25	16.53	22.20	...	22.2	No
SDSS J212413.89+010000.3	19	T5.0	16.03	16.14	22.26	...	22.3	No
2MASS J21513839-4853542	26	T4.0	15.73	15.43	22.34	...	22.3	No
2MASS J04070885+1514565	16	T5.0	16.06	15.92	22.51	...	22.5	No
SDSS J151114.66+060742.9	20	T0.0	16.02	14.54	22.67	...	22.7	No
SDSSp J092615.38+584720.9AB	18	T4.5	15.90	15.45	22.73	...	>22.7	Yes	29	binary: a=0''070

Table 9—Continued

Name of T Dwarf	Discovery Reference ^c	NIR SpT	J^a (mag)	K_s^a (mag)	Distance (pc)		Adopted Distance ^b	High-res imaging?	Follow-up Reference ^c	Remarks
					from J	from π_{trig}				
SDSS J105213.51+442255.7	20	T0.5	15.96	14.57	23.08	...	23.1	No
SDSSp J111010.01+011613.1	18	T5.5	16.34	15.13	23.12	...	23.1	Yes	29	single
SDSS J074149.15+235127.5	19	T5.0	16.16	15.85	23.61	...	23.6	No
SDSS J163022.92+081822.0	20	T5.5	16.40	16.61	23.69	...	23.7	No
SDSS J074201.41+205520.5	19	T5.0	16.19	15.23	23.99	...	24.0	No
2MASS J05103520–4208140	7	T5.0	16.22	16.00	24.31	...	24.3	No
2MASS J05185995–2828372AB	27	T1.0	15.98	14.16	24.32	...	>24.3	Yes	29	binary: a=0'051
2MASSI J2339101+135230	3	T5.0	16.24	16.15	24.50	...	24.5	Yes	29	single

^aPhotometry from 2MASS All-Sky Point Source Catalog.

^bDistance adopted from trigonometric parallax if measured.

^cReferences: (1) Scholz et al. (2003), (2) Biller et al. (2006), (3) Burgasser et al. (2002), (4) Nakajima et al. (1995), (5) Burgasser et al. (2000a), (6) Artigau et al. (2006), (7) this paper, (8) Burgasser et al. (2003a), (9) Tinney et al. (2005), (10) Burgasser et al. (2003c), (11) Burgasser et al. (2000b), (12) Burgasser et al. (1999), (13) Strauss et al. (1999), (14) Mugrauer et al. (2006), (15) Leggett et al. (2000), (16) Burgasser et al. (2004b), (17) Tsvetanov et al. (2000), (18) Geballe et al. (2002), (19) Knapp et al. (2004), (20) Chiu et al. (2006), (21) Cruz et al. in prep, (22) Luhman et al. (2007), (23) Hawley et al. (2002), (24) Kirkpatrick et al. (2000), (25) Wilson et al. (2001), (26) Ellis et al. (2005), (27) Cruz et al. (2004), (28) McCaughrean et al. (2004), (29) Burgasser et al. (2006c), (30) Golimowski et al. (1998), (31) Burgasser et al. (2003b), (32) Reid et al. (2001), (33) Burgasser et al. (2005a).

^dH-band magnitude from Biller et al. (2006).

^ePhotometry is from Luhman et al. (2007).